Testing the usefulness of optical data for zooplankton long-term monitoring: Taxonomic composition, abundance, biomass, and size spectra from ZooScan image analysis

Astrid Cornils [ORCID],[1]* Karolin Thomisch,[2] Joanna Hase,[1] Nicole Hildebrandt,[1] Holger Auel,[3] Barbara Niehoff[1]*

[1]Section Polar Biological Oceanography, Alfred Wegener Institute Helmholtz Centre for Polar and Marine Research, Bremerhaven, Germany
[2]Section Physical Oceanography of the Polar Seas, Alfred Wegener Institute Helmholtz Centre for Polar and Marine Research, Bremerhaven, Germany
[3]Universität Bremen, FB02, BreMarE—Bremen Marine Ecology, Bremen, Germany

Abstract

The pelagic ecosystem of the Arctic Ocean is threatened by severe changes such as the reduction in sea-ice coverage and increased inflow of warmer Atlantic water. The latter is already altering the zooplankton community, highlighting the need for monitoring studies. It is therefore essential to accelerate the taxonomic identification to speed up sample analysis, and to expand the analysis to biomass and size assessments, providing data for modeling efforts. Our case study in Fram Strait illustrates that image-based analyses with the ZooScan provide abundance data and taxonomic resolutions that are comparable to microscopic analyses and are suitable for zooplankton monitoring purposes in the Arctic. We also show that image analysis allows to differentiate developmental stages of the key species *Calanus* spp. and *Metridia longa* and, thus, to study their population dynamics. Our results emphasize that older preserved samples can be successfully reanalyzed with ZooScan. To explore the applicability of image parameters for calculating total mesozooplankton and *Calanus* spp. biomasses, we used (1) conversion factors (CFs) translating wet mass to dry mass (DM), and (2) length–mass (LM) relationships. For *Calanus* spp., the calculated biomass values yielded similar results as direct DM measurements. Total mesozooplankton biomass ranged between 1.6 and 15 (LM) or 2.4 and 21 (CF) g DM m^{-2}, respectively, which corresponds to previous studies in Fram Strait. Ultimately, a normalized biomass size spectra analysis provides 1st insights into the mesozooplankton size structure at different depths, revealing steep slopes in the linear fit in communities influenced by Atlantic water inflow.

In the Arctic, pelagic ecosystems are severely threatened by climate change. Sea ice thickness and extent are shrinking, and ice-free periods are prolonged (Stroeve et al. 2012; Kwok 2018). Also, the inflow of warmer Atlantic water has increased over the last decades (Beszczynska-Möller et al. 2012; Muilwijk et al. 2018), leading to higher abundances of boreal species in the Arctic Ocean (Fossheim et al. 2015; Polyakov et al. 2017; Møller and Nielsen 2019). Within pelagic communities zooplankton, particularly herbivorous copepods, are a central link between primary production and higher trophic levels (Mitra et al. 2014). Zooplankton are also of major importance for the carbon turnover and export (Wassmann et al. 2004; Riser et al. 2008; Darnis and Fortier 2012; van der Jagt et al. 2020). They contribute to the microbial loop in the surface layer, either retaining nutrients in the upper water column (Møller et al. 2003; Calbet and Saiz 2005; Møller 2005; Schnack-Schiel and Isla 2005), or enhancing the nutrient export to the deep-sea via excretion and vertical migration (Longhurst and Harrison 1988; Smetacek and Nicol 2005; Alcaraz et al. 2010). Changes in zooplankton community composition will therefore have cascading effects. Assessing population dynamics and biogeography in relation to environmental variables is essential to predict ecosystem

Author Contribution Statement: AC and BN designed the study. KT and NH performed the sampling. KT and NH conducted the microscopic analysis. JH and AC conducted the image analysis. AC performed the data analysis. AC and BN wrote the manuscript with contributions of all authors.

processes and functioning in the future Arctic. Intensive zooplankton sampling has therefore been an integral part of the monitoring program at the AWI Deep Sea Observatory Hausgarten in Fram Strait since 2011 and of the MOSAiC expedition 2019/2020 in the central Arctic Ocean, both resulting in hundreds of samples that need to be analyzed.

Traditionally, mesozooplankton organisms (0.2–20 mm) are identified and counted under a stereo-microscope. Due to the high abundance of zooplankton, the samples are usually vigorously split or sub-sampled with pipettes, and only small aliquots are analyzed (Postel et al. 2000). The digitalization of zooplankton samples with the ZooScan—a waterproof scanner to obtain images of zooplankton samples (Grosjean et al. 2004; Gorsky et al. 2010)—and the semi-automatic analysis of the images with the tool EcoTaxa (Picheral et al. 2017) have, in part, overcome these problems. This method considerably reduces the sample processing time and, thus, allows to analyze larger aliquots. Moreover, experts from all over the world can share zooplankton images since EcoTaxa is a web-based platform and thus accessible from any computer (Picheral et al. 2017). However, image-based (ZooScan) identification has resulted in relatively low taxonomic resolution, that is, at maximum to families and genera, unless the organism possesses distinct morphological features (Benfield et al. 2007). Also, developmental stages have, to our knowledge, not yet been identified on ZooScan images and thus, only stereo-microscopy has provided detailed species lists and abundances of developmental stages in the Arctic Ocean.

Reliable biomass estimates of the zooplankton community are essential to determine their importance in carbon cycling and export, and they are becoming more and more relevant for ecosystem modeling (Le Quéré et al. 2016; Villarino et al. 2018; Heneghan et al. 2020) and management (Petchey and Belgrano 2010). A major advantage of the ZooScan over microscopic analyses is that the automatic measurements of longest (major) and shortest (minor) axis of each organism allow to determine a body-size equivalent of each organism and consequently biomass estimates (Alcaraz et al. 2010; Gorsky et al. 2010). Body size is an important life-history trait as it can relate to the trophic level of an organism (Litchman et al. 2013; Kiørboe and Hirst 2014; Andersen et al. 2015). Also, individual size decreases with increasing temperature (Brun et al. 2017) and, thus, size–frequency distributions have the potential to decipher the origin of populations in terms of water masses (Basedow et al. 2010). Shifts in zooplankton size structure may even be indicative of climate change, especially of ocean warming (Daufresne et al. 2009; Atkinson et al. 2021).

In the Arctic, copepods usually comprise more than 90% of the mesozooplankton abundance (Kosobokova and Hirche 2000). Polar copepods are often larger in size compared to temperate and tropical regions (Brandão et al. 2021), which should allow to identify the organisms to a lower taxonomic level, as shown for in situ images of Arctic copepods (Schmid et al. 2016). This study therefore tested the hypotheses (i) that using the ZooScan can yield abundances and species numbers, which are similar to those obtained by microscopy, and (ii) that developmental stages of Arctic (key) copepod taxa can be identified on digital images, allowing to expand the ZooScan approach to studies on population dynamics. In addition, we explore the potential of body sizes, as automatically measured by ZooProcess, to calculate biomasses (dry mass [DM] and carbon) and to investigate the size structure of the community independent of species.

Here, we present a case study, comparing microscopic counts with digital image analyses of zooplankton at six stations in the Fram Strait. Based on vertically stratified zooplankton samples from the long-term monitoring program in Fram Strait (Soltwedel et al. 2005, 2016), we show that the level of taxonomic classification and determination of developmental stages as identified from images, matches that of microscopy, and we suggest that image analyses can, at least partly, substitute microscopical work on zooplankton biodiversity, biogeography, and population dynamics.

Material and methods

Sampling

Zooplankton was collected from 29 June 2011 to 10 July 2011 during a cruise with RV Polarstern (ARK XXVI-1) to the Fram Strait. Six stations along a transect at 78°50′N from Spitsbergen (Norway) to Greenland (Denmark) (Fig. 1; Table 1) were sampled with a MultiNet (type Midi, Hydrobios, Germany; 150 μm mesh size, 0.25 m^2 net opening) from at maximum depth of 1500 m to the surface. Standard depth intervals were 1500–1000–500–200–50–0 m, except for Stas. 71 and 127 with bottom depths < 1500 m (Table 1). In these cases, higher resolution depth intervals were sampled (Supporting Information Table S1). A digital flow meter mounted in the net opening measured the volume of filtered sea water by each of the five nets. Immediately after capture, the samples were sieved over 100 μm mesh and preserved in a 4% formaldehyde/seawater solution buffered with hexamethylenetetramine. The samples were stored at room temperature until later analysis in the laboratory. In addition, *Calanus* spp. specimens were sorted alive from vertical Bongo net hauls (0–250 m, mesh sizes 200 or 300 μm) and deep frozen to measure biomass and carbon content of their developmental stages (see below).

Hydrography

During the cruise, temperature and salinity profiles, measured with a CTD (Sea-Bird SBE 911plus), were obtained at all zooplankton stations (Beszczynska-Möller and Wisotzki 2012). For visualization, the hydrographical data were plotted with Ocean Data View vs. 5.3.0 (Schlitzer 2021), using a strong stretched projection of the upper 1000 m as most of the hydrographical variability was found in this depth layer.
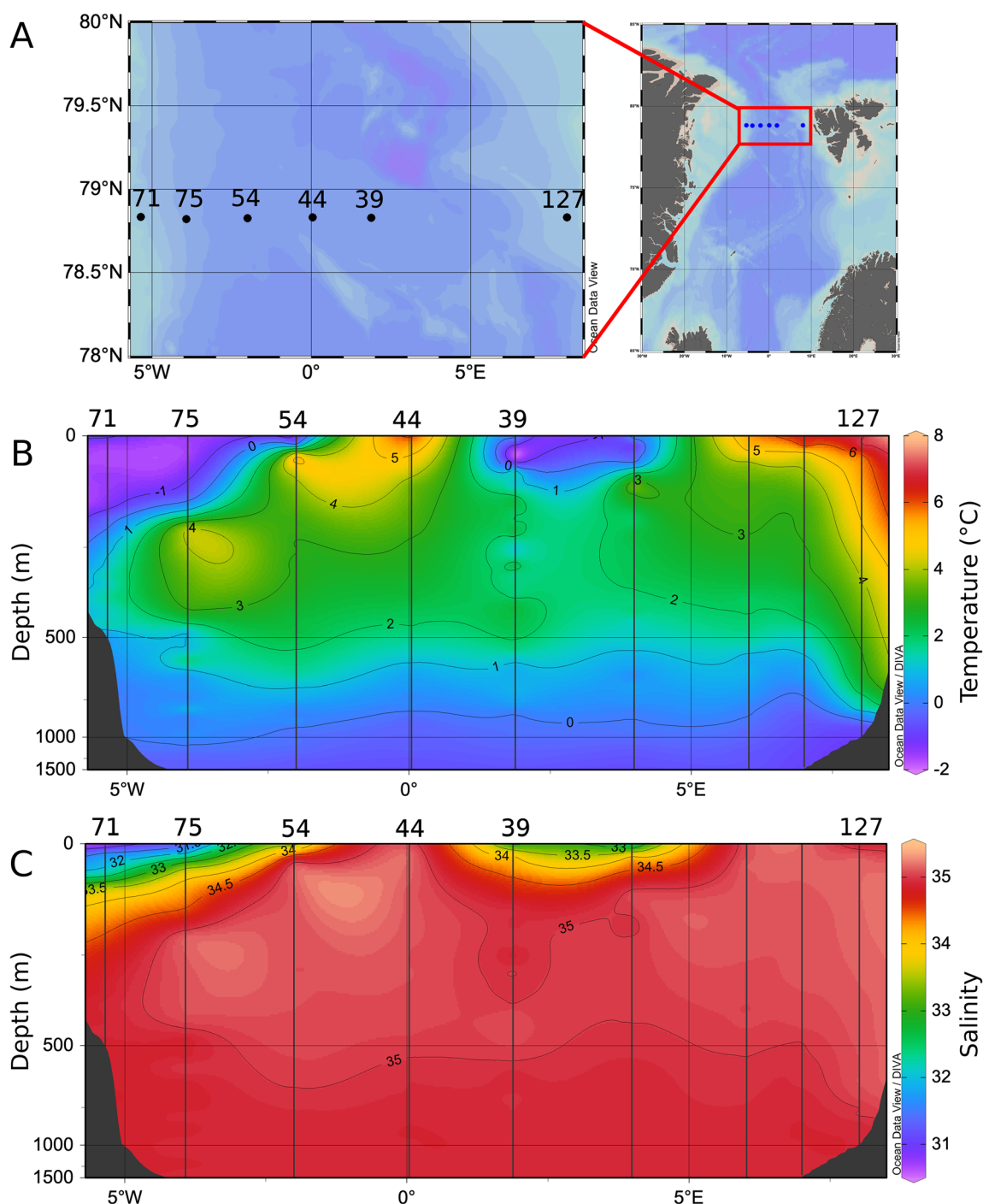
Fig. 1. Map of the transect at 78.8°N with station numbers (**a**) and plots of temperature (**b**) and salinity (**c**) with a strong stretched projection of the upper 1000 m of the water column (DIVA gridding); data derived from Beszczynska-Möller and Wisotzki (2012).

Sample analysis—microscopy

Shortly after the cruise, from October 2011 to March 2012, the samples were microscopically analyzed. All samples were split in half using a Motoda plankton splitter in the laboratories. Usually, one half was archived, and the 2nd half was split into smaller aliquots (1/4 to 1/256, Supporting Information Table S1), and then analyzed under a stereo-microscope (Leica MZ 12.5). Abundant taxa were counted from smaller aliquots

until at least 50 individuals of each taxon were determined, while rare taxa (e.g., *Paraeuchata* spp., *Scaphocalanus* spp., Amphipoda, Euphausiacea) were counted from the largest aliquot (i.e., ½) or, when abundances were extremely low, also from the aliquot allocated to archiving.

Calanoid copepods were determined to species level, if possible, while cyclopoid and harpacticoid copepods were identified to family or genus level only. In the calanoid species

Table 1. Stations along a transect across Fram Strait during the RV Polarstern cruise ARK XXVI-1.

Station no.	Latitude, °N	Longitude, °E/W	Bottom depth (m)	Date	Time UTC	Ice cover
PS78/71-5	78.834	5.329 W	722	04 Jul 2011	09 : 34	Ice covered
PS78/75-5	78.834	3.895 W	2007	04 Jul 2011	00 : 47	Ice covered
PS78/54-5	78.832	1.982 W	2715	01 Jul 2011	18 : 47	Ice margin
PS78/44-4	78.835	0.079 E	2631	29 Jun 2011	21 : 00	No
PS78/39-5	78.838	1.790 E	2558	29 Jun 2011	04 : 12	No
PS78/127-7	78.825	8.008 E	1027	10 Jul 2011	13 : 25	No

Calanus finmarchicus, *Calanus glacialis*, *Calanus hyperboreus*, and *Metridia longa* late copepodite stages 4 and 5 (CIV–CV) and adult sexes were separated. The young copepodite stages 1 to 3 (CI–CIII) were combined in *M. longa*. For the genus *Calanus*, CI - CIII of all three species were counted as "Calanidae CI–CIII". For the comparison with the ZooScan results, the respective developmental stages of the two species were combined as *C. finmarchicus/glacialis*. Copepod nauplii were not determined to genus or species level as they are not sampled quantitatively by nets of 150 μm mesh size, and likely early nauplius stages of small species are underestimated. We did include the nauplii into our analyses nevertheless as to test the applicability of microscopy and image analyses for small organisms and because the occurrence of nauplii is indicative of reproductive activity, and thus of ecological interest. Noncopepod taxa were separated into higher taxa only, for example, Ostracoda, Isopoda, Polychaeta, Bivalvia and Cnidaria due to their minor contribution to the zooplankton community.

Sample analysis—ZooScan

In 2019, the archived (sub)samples were reanalyzed with the ZooScan (Gorsky et al. 2010). The archived subsample (1/2 of the original sample) was sieved over 500 μm mesh to size-fractionate the sample which facilitates the semi-automatic annotation (see below). The fraction <500 μm was stained with Rose Bengal to enhance the contrast of small organisms on the images. Each size fraction was split with a Motoda plankton splitter into aliquots up to 1/16. This was sufficient to obtain approximately the recommended number of objects (Gorsky et al. 2010) to provide the optimal scanning success (up to 1500 images in the size fraction >500 μm and ~2000 images for the size fraction <500 μm for the standard threshold). These subsamples were then processed with the ZooScan (Biotom, Hydroptic, France).

Following Gorsky et al. (2010), we carefully filled the scanning area with freshwater and applied the scanning frame (15 * 24 cm). First, for background subtraction, we scanned the blank background using VueScan (version 8.3.23). Then, we transferred the sample into the scanning frame, manually separated overlapping individuals and scanned the sample at a resolution of 2400 dpi. The scans were processed with ZooProcess (version 7.29), a macro in ImageJ (Schneider

et al. 2012), to extract images with single individuals, to measure each individual, and to link each object with associated metadata. All images were uploaded to the web application EcoTaxa (Picheral et al. 2017). For semi-automatic prediction, a training set of taxonomic categories according to the data from the microscopic analysis (Tables 6, 7) was built by manually classifying up to 200 random images per taxonomic category from all samples. Based on this training set, the identity of all remaining objects was predicted using the Random Forest algorithm provided by EcoTaxa. The predictions were manually either validated or corrected. In total, approximately 200,000 objects were identified. Among these, approximately 66,000 (33%) grouped into detritus/artifacts, feces, bubbles, or eggs, and were excluded from the data set. Approximately, 800 images showed 2 or more organisms which were identified and counted manually. The measurements that were necessary for biovolume and biomass estimates (major/minor axis, description see below) for the objects on these images were obtained from the mean values of all individuals of the respective taxon from the same sample and size fraction, or in the case of rare taxa from all samples of the same station.

Species identification was difficult, if relevant morphological diagnostic characteristics were not visible on the image due to the orientation of the organism on the image or if images were blurred. Organisms on such images were identified to the lowest taxonomic level possible (e.g., Augaptilidae, Lucicutiidae, Calanoida, Euphausicacea, unidentified Copepoda).

Images of *Calanus* specimens were sorted manually into the categories *C. finmarchicus/glacialis* and *C. hyperboreus* and separated into adults (female/male) and developmental stages (CI–CV). *Calanus* specimens, in which species/developmental stages could not be identified, were grouped as "*Calanus* spp." (33 of 14,308 *Calanus* images). Images of *M. longa* were also separated manually according to their sex and developmental stage. For the comparison with the microscopic analysis the young stages CI–CIII were grouped for *Calanus* spp. and *M. longa*, respectively (Fig. 2).

The image parameters associated with each individual image include variables for shape and size (Gorsky et al. 2010; Vandromme et al. 2012). Among others, they describe the primary ("major") and the secondary ("minor") axis of the best
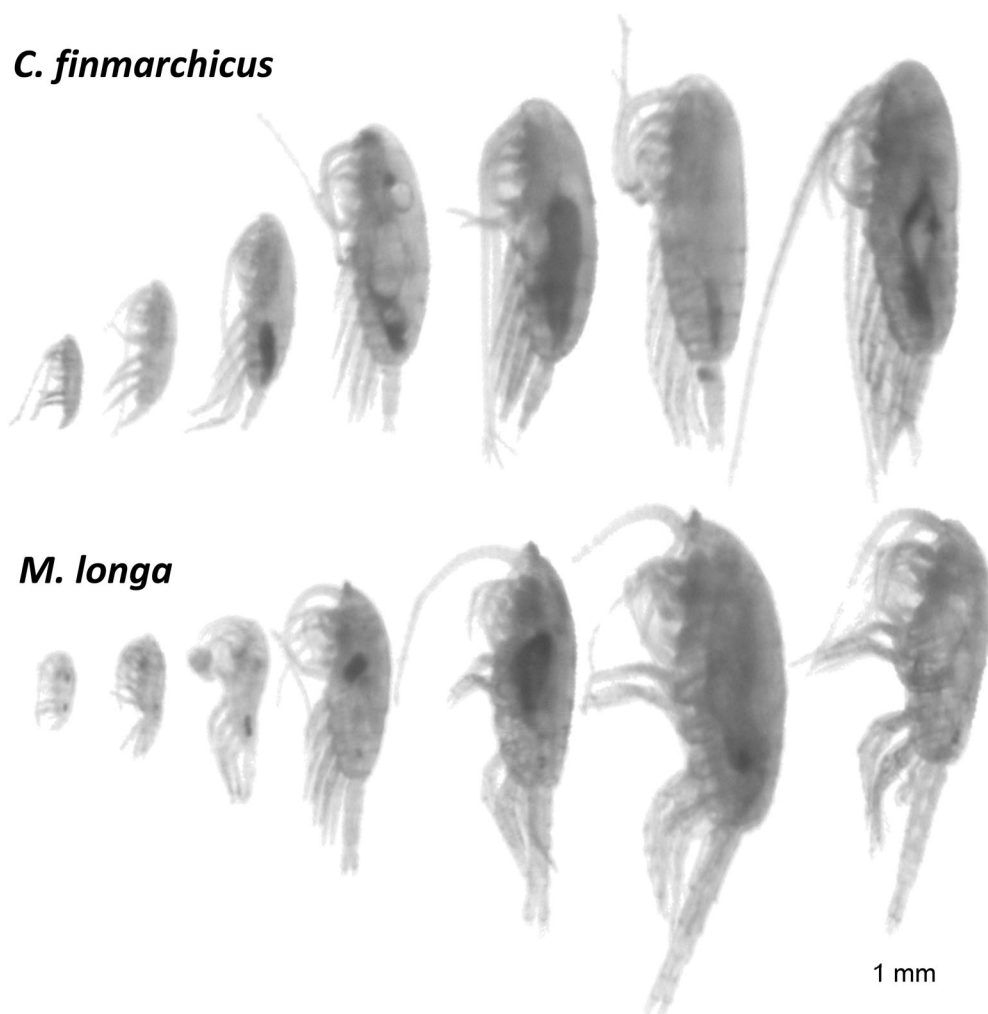
Fig. 2. Juvenile and adult stages of *Calanus finmarchicus* and *Metridia longa* on ZooScan images. From left to right: Copepodite stages 1–5 (CI–CV), female and male.

fitting ellipse of the objects. With these two values, the equivalent spherical diameter (ESD; mm) for an elliptical body was calculated as an equivalent for body size (ESD = 2 *$\sqrt{}$(major/2 * minor/2)), and the biovolume (BV; mm^3) of each individual (BV = 4/3 * π * (major/2*(minor/2)^2)). The formula was used to account for the ellipsoid shape of copepods, the numerically dominant zooplankton in our samples. The biovolume of each taxonomic category was then calculated as the sum of the biovolumes of all individuals in that category divided by the volume of filtered water (BV: mm^3 m^{-3}).

Adjustment of image processing

At an early stage of our ZooScan analyses, we observed that the abundances of large calanoid taxa (e.g., *Calanus* spp., *M. longa*) derived from digital images matched those derived from microscopy, but the abundances of small-sized organisms (<1 mm length) were considerably lower when calculated based on ZooScan image counts. This had severe

consequences for the community composition due to the underestimation of small-sized taxa or groups (e.g., *Oithona* spp., *Microcalanus* spp., Oncaeidae, Nauplii).

As a standard, ZooProcess sets a 300 μm minimum ESD, that is, only images with objects $> 300\,\mu$m ESD were extracted from the scanned image. To match the mesh size of the Multinet, we set the minimum ESD to 150 μm. Lowering the minimum ESD increased the numbers of small sized copepod taxa and led to similar abundances as in microscopic counts, and thus all scans were processed using the lower threshold.

Generally, the number of echinoderms and mollusk larvae was much lower in ZooScan counts as compared to microscopic counts. At close inspection, their shells and skeletons were greatly dissolved at the time of the reanalysis (8 years after collection), possibly due to pH changes in the preserved samples. Hence, we removed mollusks (except for *Clione limacina*) and echinoderms from our data analyses, but note

Table 2. Linear relationships ($y = a + b * x$) between ESD and PL for Copepoda and ESD and TL for other zooplankton taxa.

Taxon	a	b	R^2	Taxon	a	b	R^2
Copepoda*	0.031	1.2	0.99	Crustacea†	0.064	1.7	0.99
Calanoida*	0.038	1.2	0.99	Amphipoda	0.17	1.5	0.98
Euchaetidae	0.081	1.2	1	Euphausiacea	0.34	2	0.98
Aetideidae	0.17	1.1	0.98	Ostracoda	0.097	1.4	0.99
Clausocalanidae	0.09	1.4	0.94	Appendicularia	0.074	0.59	0.68
Scolecitrichidae	0.03	1.3	0.98	Chaetognatha	0.25	4.2	0.98
Spinocalanidae	0.063	1.3	0.98	Cnidaria	0.22	0.9	0.89
Metridinidae	0.051	1.2	0.9	Polychaeta	0.22	1.9	0.9
Heterorhabdidae	0.004	1.2	0.98	Other zooplankton‡	0.14	1	0.81
Calanus hyperboreus	0.23	1.3	0.99				
Calanus finmarchicus/Calanus glacialis	0.29	1.3	0.98				

*Without *Calanus*.
†Without Copepoda.
‡Without *Chaetognatha*.

here that, when present, these organisms can be identified on the ZooScan images.

Length estimates as a prerequisite to calculate DM from images

The ESD is an equivalent for body size calculated from image parameters. Many length–mass (LM) relationships for copepods however, are based on the prosome length (PL) instead of total length (TL). Furthermore, other zooplankton such as amphipods or chaetognaths are often bent on images and thus, the ESD might differ from the actual length measure used in LMs. To obtain a more accurate analysis of PL of copepods and TL of other zooplankton, we therefore measured the respective body length of 40 randomly selected images from each taxonomic category in ImageJ using a segmented line to account for bent organisms. In total, 2815 individuals were measured. The measured body length was then plotted against the ESD to establish a linear least square regression (Table 2) for different zooplankton taxa (Supporting Information Fig. S1). Significant relationships could be established for several calanoid copepod families as well as for other zooplankton taxa (Table 2). To calculate ESD length

Table 3. CFs from WM (mg) to DM (mg) for Arctic zooplankton taxa used in the present study.

Taxa	Original taxon	CF	SD	References
Arctic Copepoda		0.162	0.024	Kosobokova and Hirche (2000)
Aglantha digitale		0.053	0.001	Ikeda and Skjoldal (1989)
Gastropoda	*Limacina helicina*	0.222	0.008	Ikeda and Skjoldal (1989)
Clione limacina	<50 mg DM	0.058	0.01	Ikeda and Skjoldal (1989)
Parathemisto spp.	*Parathemisto libellula*	0.176	0.016	Ikeda and Skjoldal (1989)
Euphausiacea	*Thysanoessa inermis* (<10 mg DM)	0.259	0.018	Ikeda and Skjoldal (1989)
Cnidaria		0.041	0.003	Kiørboe (2013)
Polychaeta	*Tomopteris* sp.	0.139		Kiørboe (2013)
Crustacea		0.183	0.019	Kiørboe (2013)
Amphipoda		0.239	0.09	Kiørboe (2013)
Ostracoda	Large *Conchoecia* spp.	0.159		Kiørboe (2013)
Chaetognatha	*Eukrohnia hamata*	0.077		Kiørboe (2013)
Tunicata		0.054	0.019	Kiørboe (2013)
Other zooplankton	Zooplankton	0.2		Postel et al. (2000)
Calanus finmarchicus	Female *C. finmarchicus*	0.245	0.01	Ikeda and Skjoldal (1989)
Calanus glacialis	Female *C. glacialis*	0.234	0.01	Ikeda and Skjoldal (1989)
Calanus hyperboreus	Female *C. hyperboreus*	0.32	0.038	Ikeda and Skjoldal (1989)

relationships for taxa with nonsignificant regressions and rare taxa, all measured specimens were grouped in the overarching categories Calanoida, Copepoda, other Crustacea and other zooplankton. For the linear regressions of Calanoida and Copepoda, all *Calanus* spp. and their developmental stages were excluded as they were highly over-represented in the data set of measured length, accounting for 15 taxonomic categories within the Copepoda. Chaetognatha were excluded from the group of other zooplankton because their regression line differed greatly from those of other non-Crustacean zooplankton (Supporting Information Fig. S1).

DM estimates

Both biovolume and size can be used to derive biomass by applying either conversion factors (CFs) from wet mass (WM) to DM (Ikeda and Skjoldal 1989; Kiørboe 2013; Bode et al. 2018; Pitois et al. 2021; Maas et al. 2021a) or established LM relationships in combination with abundance (Richter 1994; Hopcroft et al. 2004; Liu and Hopcroft 2008; Nakamura et al. 2017). Here, we apply these approaches and in the case of *Calanus* spp. compare the results with biomass estimates from mean DM data measured directly during this study or from previous publications (Table 5).

(1) Conversion from biovolume to DM: The biovolume of each individual (mm^3) is converted to WM (mg) by assuming that the preserved zooplankton organisms are neutrally buoyant with a specific density of 1 g cm^{-3} (Postel et al. 2000 and references therein). In zooplankton, DM generally accounts for 5% to 20% of WM. Hereinafter, the fraction of DM in relation to WM is given as CF. For Copepoda, a general CF of 0.16 for Arctic copepods was applied (Kosobokova and Hirche 2000). Several CFs for other Arctic zooplankton taxa

Table 4. LM relationships for Arctic zooplankton taxa.

Taxon	Original taxon	c	d	DM m^{-3}	Formula	References
Cnidaria	*Aglantha digitale*	0.0019	3.05	DM mg	$c * TL^d$	Matthews and Hestad (1977)
Clione limacina		0.0222	2.438	DM mg	$c * TL^d$	Mizdalski (1988)
Gastropoda	*Limacina helicina*	0.1679	1.361	DM mg	$c * TL^d$	Mizdalski (1988)
Polychaeta	*Tomopteris* sp.	0.005	2.25	DM mg	$c * TL^d$	Matthews and Hestad (1977)
Amphipoda	*Parathemisto libellula*	0.006	2.822	DM mg	$c * TL^d$	Auel and Werner (2003)
Chaetognatha	*Eukrohnia hamata*	0.041	0.165	DM mg	$c*e^{(TL^d)}$	Richter (1994)
Appendicularia	*Fritillaria pellucida*	3.21	9.11	logDM μg	$c * logTL^{-d}$	Hopcroft et al. (2004), from Fenaux (1976)
Ostracoda		0.033	2.37	DM mg	$c * TL^d$	Richter (1994)
Euphausiacea/Mysida	*Thysanoessa inermis*	2.5	1.162	logDM mg	$c * logTL^{-d}$	Pinchuk and Hopcroft (2007)
Calanus finmar-chicus/Calanus glacialis	*Calanus finmar-chicus/ glacialis*	0.029	2.693	DM mg	$c * PL^d$	Present study
Calanus hyperboreus		0.040	2.285	DM mg	$c * PL^d$	Present study
Heterorhabdidae	*Heterorhabdus norvegicus*	0.003	4.716	DM mg	$c * PL^d$	Richter (1994)
Metridinidae/Lucicutiidae	*Metridia longa*	0.012	3.017	DM mg	$c * PL^d$	Hirche and Mumm (1992)
Aetideopsis spp.	*Aetideopsis* spp.	0.005	4.659	DM mg	$c * PL^d$	Richter (1994)
Aetideidae	*Chiridius/Gaetanus* spp.	0.01	3.412	DM mg	$c * PL^d$	Richter (1994)
Pseudocalanus spp.	*Pseudocalanus* spp.	2.85	7.62	logDM μg	$c * logTL^{-d}$	Liu and Hopcroft (2008)
Microcalanus spp.	*Microcalanus* spp.	2.85	7.62	logDM μg	$c * logTL^{-d}$	Liu and Hopcroft (2008)
Paraeuchaeta spp.	*Paraeuchaeta* spp.	0.008	3.274	AFDM mg	$c * PL^d$	Mumm (1991)
Scaphocalanus spp.	*Scaphocalanus magnus*	10.69	3.341	DM μg	$c * PL^d$	Yamaguchi et al. (2020)
Scolecithricella minor	*Scolecithricella minor*	3.669	9.739	logDM μg	$c * logPL^{-d}$	Nakamura et al. (2017)
Cyclopoida	Cyclopoida	1.997	5.325	logDM μg	$c * logPL^{-d}$	Nakamura et al. (2017)
Poecilostomatoida	Poecilostomatoida	2.875	7.458	logDM μg	$c * logPL^{-d}$	Nakamura et al. (2017)

AFDM, ash-free dry mass, assuming ca. 90% of DM (Kjørboe 2013).

from the Barents Sea were used (Table 3; Ikeda and Skjoldal 1989). Additional CFs for higher taxa were taken from a review on zooplankton body composition (Kiørboe 2013 and references therein). For all other Arctic zooplankton taxa, a general CF of 0.2 was applied (Postel et al. 2000).

Ikeda and Skjoldal (1989) also published CFs for each of the three Arctic *Calanus* species that were higher compared to the general CF for Arctic copepods. To investigate the impact of the CF on the estimated DM, the species-specific CFs as well as the general CF for Arctic copepods were applied for *Calanus* spp. (Table 3).

(2) LM relationships: Established LM relationships for Arctic taxa were used to estimate individual DM (mg) (Table 4). When no LM relationships from Arctic organisms were available, relationships for sub-Arctic (Nakamura et al. 2017) or Antarctic sister species (Mizdalski 1988) were applied. The body or PL calculated with the linear ESD–length relationships (Table 2) was used as length measure. For *Calanus* spp., LM relationships were calculated from direct measurements of DM (mg) and PL (mm) obtained during the present study for females, CV stages and CIV stages (only *C. hyperboreus*), and from Gluchowska et al. (2017) for CI–CIV stages (see Table 5; Supporting Information Fig. S1). For taxonomic categories not mentioned in Table 4, no suitable LMs were found (e.g., unidentified copepods, nauplii, Isopoda, Spinocalanidae, Mormonilloida). These taxa were converted to individual DM (mg) with factors as described above for Copepoda and other zooplankton (Table 3).

(3) DM measurements of *Calanus* spp.: At each station, up to 12 individuals per species and life stage (CIV, CV, female)

of *Calanus* spp. were sorted onboard from Bongo net samples. In total, 384 individuals were collected (Table 5). Their PL was measured onboard under a stereo-microscope (magnification: 16–32 folds, error between 0.03 and 0.06 mm). Afterward, each individual was rinsed with deionized water and transferred to a pre-weighted tin cap and stored at $-20°C$. The copepod samples were then dried at $60°C$ for at least 48 h and weighted to measure individual DM (mg). As in preserved sample analyses, the three *Calanus* species were distinguished based on their PL (Unstad and Tande 1991). For the smaller copepodite stages CI–CIV published DM data were used (Table 5).

Normalized biomass size spectra

Normalized biomass size spectra (NBSS) have the potential to detect patterns in the pelagic community structure in relation to environmental parameters (Basedow et al. 2010; Lampe et al. 2021). To assess spatial and vertical differences in zooplankton biomass size spectra, NBSS were calculated from individual biovolumes ($mm^3 \, m^{-3}$) for each sample. For comparison with other stations, samples from the shallow Stas. 71 and 127 were merged to the standard depth intervals 500–200–50 m (Supporting Information Table S1).

According to the method of Sprules and Barth (2016), the biovolume of each individual was sorted into octave-scale size classes, starting with the lowest biovolume size class at $0.0000155 \, mm^3 \, m^{-3}$, and then each following size class was doubled. Thus, intervals with small biovolume size classes were narrow, while larger size classes increased in width. The

Table 5. Mean individual PL and DW of developmental stages of *Calanus* spp.; in CIV stages (only *Calanus hyperboreus*), CV stages and females PL and DM were measured during the present study. For the younger CI–CIV stages, PL and DM were obtained from the literature (Gluchowska et al. 2017 and references therein).

Species	Stage	*n*	PL (mm; mean $\pm$ SD)	DM (mg ind^{-1})
Calanus finmarchicus	CI		0.680	0.005
	CII		0.926	0.011
	CIII		1.315	0.029
	CIV		1.734	0.075
	CV	84	2.680 $\pm$ 0.105	0.499 $\pm$ 0.167
	f	84	2.790 $\pm$ 0.155	0.416 $\pm$ 0.142
Calanus glacialis	CI		0.927	0.009
	CII		1.306	0.022
	CIII		1.813	0.062
	CIV		2.481	0.198
	CV	13	3.274 $\pm$ 0.217	0.640 $\pm$ 0.322
	f	23	3.675 $\pm$ 0.239	0.987 $\pm$ 0.268
Calanus hyperboreus	CI		1.039	0.0011
	CII		1.633	0.029
	CIII		2.474	0.112
	CIV	24	3.306 $\pm$ 0.367	0.347 $\pm$ 0.192
	CV	89	4.672 $\pm$ 0.522	1.393 $\pm$ 0.723
	f	66	6.530 $\pm$ 0.277	2.929 $\pm$ 1.136

biovolume of all individuals within one size class was summed up to obtain the total biovolume per size class. To normalize the total biovolume, it was divided by the width of the size class and then was $\log_2$ transformed. To visualize the NBSS, the normalized total biovolume was plotted against the normalized ($\log_2$) midpoint of the corresponding size class interval (Sprules and Barth 2016; Plum et al. 2021).

The smallest size classes obtained with the ZooScan often show minima that reflect the detection limit of the instrument, that is, the threshold for image extraction (García-Comas et al. 2014). In our case, the smallest size classes match the mesh size, and such size classes are not retained quantitatively (Lombard et al. 2019). To avoid such sampling bias, we excluded the 1st two size classes for the calculation of the least-squares linear regressions.

To interpret the results of the NBSS, the slope of the negative linear biomass-size relationship is used (Plum et al. 2021). The slope reflects the relative dominance of small vs. large individuals in a community for overall biomass, that is, the steeper the curve the higher is the relative abundance of small individuals (high small : large size ratio). Furthermore, it is assumed that a linear fit (R^2) close to 1 reflects a stable community close to the steady state equilibrium. Lower or higher R^2 values indicate an unstructured and unstable community (Sprules and Munawar 1986; Zhou 2006; Sprules and Barth 2016).

Data analysis

Abundances (number of individuals m^{-3}) were calculated for all species, genera and higher taxa based on microscopic and image counts and data from the flowmeter. Biomasses (mg DM m^{-3}) based on CFs and LM relationships were calculated as the sum of all individual DMs (mg) per taxon in a sample divided by the volume of filtered water.

All data and statistical analysis were performed in the programming language R in the RStudio environment (R Core Team 2021; RStudio Team 2021). Generally, data transformation and cleaning were performed with the R package "tidyverse" (Wickham et al. 2019), graphics were visualized with "ggplot2" (Wickham 2016) and "ggpubr." Zooplankton abundances, biovolume and estimated DM were $\log_2$-transformed to reduce skewness. Linear regressions using the linear model function "*lm*" of least squares regression were conducted to compare different methods for abundance (ZooScan vs. microscopy) and to evaluate the relationship between biovolume with the different biomass estimates (i.e., CFs, LM relationships, direct measurements). Furthermore, linear regressions were used to estimate body lengths of all individuals, and for the identification of *C. finmarchicus/ glacialis* individuals from length–ESD relationships (Supporting Information Fig. S1). Nonlinear regressions were conducted for LM relationships of *Calanus* spp. using power fit curves (Supporting Information Fig. S2).

Data archiving

Image parameters, length measurements, and DM estimates for all individuals, DM measurements of *Calanus* spp., and abundance (ind m^{-3}), biovolume (mm^3 m^{-3}) and biomass (mg DM m^{-3}) for each taxonomic zooplankton category are available at the scientific database PANGAEA (Cornils et al. 2022). Single object images are stored at the web application EcoTaxa in the open access project (https://ecotaxa.obs-vlfr.fr/ prj/2771). R scripts to calculate abundance, biovolume, and biomass from the output of the EcoTaxa dataset are stored at GitHub (Cornils 2022).

Results

Hydrography

In western Fram Strait, the surface water was characterized by Polar Water ($T < 0°C$ and $S < 34.4$; after Swift and Aagaard 1981) of the East Greenland Current (Sta. 75: 0 to approximately 200 m, Sta. 71: 0 to approximately. 400 m, see Fig. 1). In eastern Fram Strait, the West Spitsbergen Current with $T > 5°C$ prevailed (Sta. 127). Atlantic Water influence ($T = 2–5°C$, $S = 34.9–35$) was strong between 200 and 500 m depth at all stations, except for Sta. 71, where colder water ($-1°C$ to $2°C$) prevailed. At Stas. 44 and 54, in the center of Fram Strait, Atlantic Water extended to the surface. Sta. 39 was located in cold ($T < 1°C$) and less saline ($S < 34.5$) water which may be attributed to Polar Water influence and ice melting processes. Below the Atlantic Water body, Return Atlantic Intermediate Water ($T = 0°C$ to $2°C$, $S = 34.9–35.0$; Paquette et al. 1985) was present down to approximately 1000 m water depth, and below that the water was cold ($T < 0°C$) and the salinity was >34.9, which is indicative of Arctic Deep Water. Sta. 127 was clearly located in the West Spitsbergen Current with water temperatures of >5°C from the surface to 200 m depth. Our samples thus originate from all different water masses typically found in Fram Strait.

Taxonomic composition and total abundance

The number of taxa and their abundances as obtained by microscopy and ZooScan image analysis were similar. Copepods were always the most abundant group, and among these, we identified 43 categories by microscopy and 41 categories by ZooScan analyses (Tables 6, 7). The non-copepod taxa were distinguished into 31 categories under the microscope and into 33 categories with the ZooScan. Non-copepod taxa usually accounted for less than 10% of total zooplankton abundance (ZooScan: mean 3.3% [range 0.2–20%]; microscopy: mean 3.5% [range 0.5–11%]). Highest contributions of noncopepods were found below 200 m water depth at Sta. 39 by image analysis (Fig. 3a,b).

With some exceptions, the categories from the two methods represented the same taxa, including species, genera, families, orders, and phyla. The main difference was that we could not determine all copepods on images to lower

Table 6. Taxa identified with via ZooScan and microscopy.

Phyla	Taxonomic categories	Z	M
Cnidaria	Cnidaria, unidentified	×	×
	Aeginidae	×	
	Solmundella bitentaculata	×	×
	Aglantha digitale	×	
	Atolla tenella	×	×
	Botrynema ellinorae	×	×
	Rhabdoon reesi	×	×
	Sminthea arctica	×	×
	Siphonophorae	×	×
Ctenophora	Unidentified	×	
	Beroe cucumis		×
Mollusca	Bivalvia, larvae	×	×
	Gastropoda, larvae	×	×
	Clione limacina	×	
Annelida	Polychaeta, unidentified	×	×
	Pelagobia cf. *longicirrata*	×	
	Typhloscolex cf. *muelleri*	×	
	Tomopteris sp.	×	
Arthropoda	Crustacea, larvae		×
	Cyclocaris guilelmi	×	×
	Lanceola clausi	×	×
	Themisto abyssorum	×	×
	Themisto libellula	×	×
	Hymenodora glacialis	×	×
	Euphausiacea, larvae*	×	×
	Euphausiacea, juv./adults	×	
	Meganyctiphanes norvegica		×
	Thysanoessa sp.		×
	Isopoda	×	×
	Ostracoda	×	×
Echinodermata	Larvae	×	×
Chaetognatha	*Eukrohnia hamata*	×	×
	Parasagitta elegans	×	
Tunicata	Fritillariidae	×	×
	Oikopleuridae	×	×
Unknown	Unidentified	×	×

*With ZooScan Euphausiacea larvae were separated in metanauplii, calyptopis, and furcilia.

taxonomic levels and therefore grouped them as "unidentified Copepoda." This category accounted on average for 7.1% (range 2.2–16.2%) of the total zooplankton abundance in image-based data, while all copepods were determined at least to the family level with microscopy (Fig. 3a,b). Also, juveniles and adults of the Euphausiacea were microscopically identified to species level, which was not possible on images since species-specific morphological features were not visible (Table 6). For the same reason, more copepod species were found under the microscope than on images. For example, on images we were able to assign specimens of the Augaptilidae

Table 7. Copepod taxa identified with via ZooScan and microscopy.

Copepod order/family	Taxonomic category	Z	M
Copepoda	Copepoda, unidentified	×	
	Copepoda nauplii	×	×
	Calanoida, unidentified	×	×
Aetideidae	Copepodite stages	×	
	Aetideopsis minor		×
	Aetideopsis rostrata	×	×
	Chiridius obtusifrons	×	×
	Gaetanus brevispinus	×	×
	Gaetanus tenuispinus	×	×
	Pseudochirella spectabilis	×	×
Augaptilidae	Augaptilidae, unidentified	×	
	Augaptilus glacialis		×
	Euaugaptilus hyperboreus		×
	Haloptilus acutifrons		×
Bathypontiidae	*Temorites brevis*	×	×
Calanidae	*Calanus finmarchicus**	×	×
	*Calanus glacialis**	×	×
	*Calanus hyperboreus**	×	×
Clausocalanidae	*Microcalanus* spp.	×	×
	Pseudocalanus spp.	×	×
Discoidae	*Disco* sp.		×
Euchaetidae	*Paraeuchaeta* spp.	×	×
	Paraeuchaeta barbata	×	×
	Paraeuchaeta glacialis	×	×
	Paraeuchaeta norvegica	×	×
Heterorhabdidae	*Heterorhabdus norvegicus*	×	×
	Paraheterorhabdus compactus	×	×
Lucicutiidae	*Lucicutia* spp.	×	×
Metridinidae	*Metridia longa**	×	×
	Metridia lucens	×	×
	Pleuromamma spp. (*robusta*)	×	×
Rhincalanidae	*Rhincalanus nasutus*		×
Scolecitrichidae	*Scpahocalanus* spp. (*brevicornis*)	×	×
	Scaphocalanus magnus	×	×
	Scolecithricella minor	×	×
	Scolecitrichopsis polaris	×	
Spinocalanidae	*Spinocalanus antarcticus*	×	×
	Spinocalanus elongatus	×	×
	Spinocalanus longispinus	×	×
	Spinocalanus longicornis	×	×
	Spinocalanus polaris		×
Tharybidae	*Tharybis groenlandica*	×	
	Undinella oblonga		×
Oithonidae	*Oithona atlantica*	×	×
	Oithona similis	×	×
Oncaeidae	Oncaeidae	×	×
Harpacticoida	*Microsetella* spp.	×	×
	Harpacticoida	×	
Mormonilloida	Mormonilloida	×	×

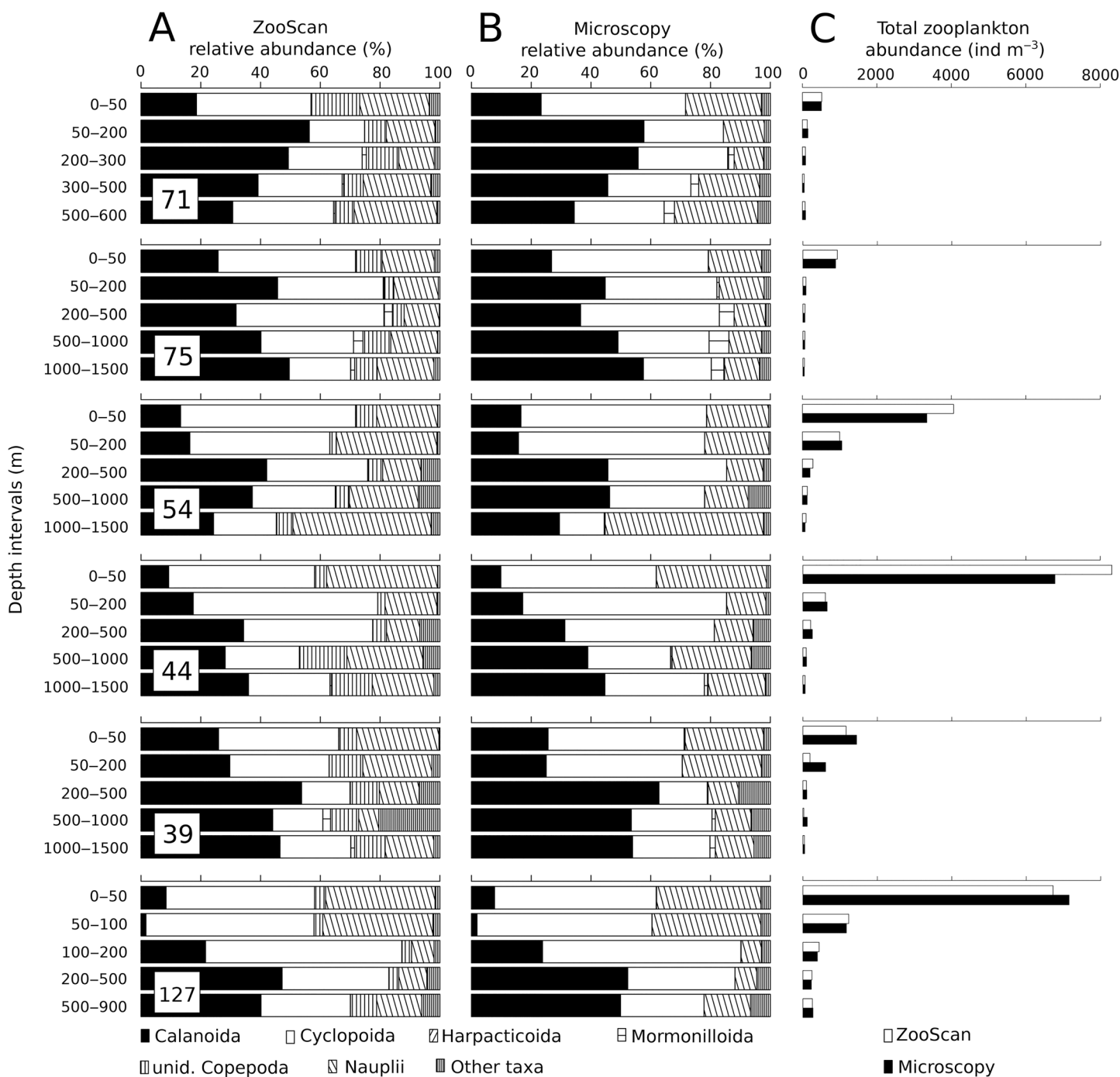*Developmental stages were separated.

Fig. 3. Relative abundances (%) of major zooplankton taxa, in particular copepod orders with ZooScan (**a**) and microscopy (**b**) derived data from six stations in Fram Strait, and total zooplankton abundances (ind m^{-3}) for both methods (**c**).

only to family level, but microscopic analyses revealed that there were in fact three species (Table 7). On the other hand, we separated developmental stages of euphausid larvae (i.e., metanauplius, calyptopis, furcilia) and identified three planktonic polychaeta species on images, but not by microscopy (Table 6), simply because the taxonomic expertise was

not available at the time of microscopic analyses. Copepod species that occurred only once or twice in the entire sample set (*Disco* spp., *Rhincalanus nasutus*, *Scolecitrichopsis polaris*, *Spinocalanus polaris*, *Tharybis groenlandica*, *Undinella oblonga*) were only found with either one of the methods, suggesting that also the imaging approach allows for the detection of rare

species, if morphological characteristics are visible and the taxonomic expertise is available.

Similar zooplankton distribution patterns emerged from both datasets (Fig. 3a,b). Total abundances were always the highest in 0–50 m (Fig. 3c), and among the stations, differed with water mass characteristics in the surface layer. Maximum abundances in the surface layer were found at Sta. 44 (ZooScan: 8300 ind m^{-3}, microscopy: 6700 ind m^{-3}) and at Sta. 127 (6700 ind m^{-3} and 7150 ind m^{-3}, respectively), characterized by warm surface water. Intermediate abundances were found at Sta. 54 (ZooScan 4062 ind m^{-3}, microscopy 3343 ind m^{-3}), while abundances in the surface layer were low (<1700 ind m^{-3}) at stations with cold Polar Surface Water (Stas. 71, 75, and 39). In the surface layer of all stations, cyclopoid copepods, in particular Oithonidae, dominated in abundance.

With depth, mesozooplankton abundance decreased considerably at all stations independent of the method (Fig. 3c). Between 50 and 200 m, it ranged from 500 to 1300 ind m^{-3} in the central and eastern Fram Strait (Stas. 54, 44, 39, and 127) and, again, cyclopoid dominated the community. At the two western Stas. 71 and 75, abundances in this depth interval were considerably lower (<130 ind m^{-3}), and here calanoid copepods were more frequent than cyclopoid copepods.

In the depth range between 200 and 500 m, the abundances decreased further at all stations in both microscopic and ZooScan analyses, ranging from 50 to 280 ind m^{-3}. At Stas. 75 and 44, cyclopoid copepods of the family Oncaeidae dominated the community. At the other four stations (71, 54, 39, 127), calanoid copepods were predominant. In the samples below 500 m depth, the abundances were also low ranging between 40 and 160 ind m^{-3}, except for Sta. 127 with 250 ind m^{-3}, and calanoid copepods prevailed except at Sta. 71. At this shallow station (600 m) in the western Fram Strait, the results of the two methods differed with cyclopoid copepods (Oncaeidae) being more abundant than calanoid copepods in the image analysis (37% and 30%) and less frequent in the microscopic analysis (30% and 34%). Possibly, the discrepancy is based on the presence of small unidentified Calanoida in the category "Unidentified Copepoda" in the image analysis.

Comparison of abundances between ZooScan and microscopy

The total zooplankton abundances of the samples from 6 stations (30 samples) derived from image analysis and microscopic counts were significantly correlated ($R^2 = 0.94$, $p > 0.0001$; Fig. 4). It is noteworthy that the abundance ratio of the two methods was close to 1 : 1 for total zooplankton, for the abundant families Calanidae and Oithonidae, and also in the less abundant Metridinidae. For *Microcalanus* spp. and Oncaeidae the explanatory power of R^2 (0.7) was lower than in the other abundant copepod taxa. *Microcalanus* spp. was the smallest calanoid copepod found in the samples, and many of the copepodite stages CI

and CII have probably been categorized as unidentified copepods by the image analysis. Furthermore, the abundance range across samples in these two taxa was narrower than in Oithonidae and Calanidae, in which abundances ranged from close to zero in deeper waters to high abundances in surface waters. Also, in the less abundant non-copepod taxa such as Chaetognatha, Appendicularia, and Ostracoda, the linear correlation between the abundance of both methods was significant with, however, less explanatory power in Ostracoda than in the other taxa. Of the 30 samples, only 2 samples from Sta. 39 (50–200 m, 500–1000 m) differed greatly from the 1 : 1 ratio in total zooplankton, with higher abundances in microscopy counts than with image analysis (Fig. 3c).

Developmental stages could be determined on images of all large calanoid copepod taxa, including *Calanus*, *Metridia*, *Paraeuchaeta*, *Heterorhabdus*, *Scaphocalanus*, and Aetideidae. In small copepods, such as *Microcalanus*, *Spinocalanus*, and *Pseudocalanus*, we were able to identify females and males on images, but not to decipher copepodite stages. The accuracy in determining developmental stages on images was therefore only addressed in *Calanus* spp. and in *M. longa* as abundances of most stages were comparably high. In developmental stages of *Calanus* spp., the linear relationships between abundances from image and microscopic analyses were significant and close to a ratio of 1 : 1 (Fig. 5), except for males of *C. finmarchicus/glacialis*. Males, however, were rare (<1.5 ind m^{-3}). The linear relationships were not as clear for the developmental stages of *M. longa*. In this taxon, high R^2 values were only found for the young CI–CIII stages (R^2: 0.81; Fig. 5).

From image parameters to DM (biomass): A comparison of approaches

For each depth stratum, *C. finmarchicus/glacialis* and *C. hyperboreus* biomass was calculated from image parameters and compared to biomass values derived from DM measurements (Fig. 6). Interestingly, biomass estimates from LM relationships based on PL (Table 2) and those based on the general CF for Arctic copepods (Table 3) yielded closest values to the measured biomass for *C. finmarchicus/glacialis*. For *C. hyperboreus* biomass estimates from LM relationships based on PL were closely related to measured biomass, while biomass estimates based on CFs for Arctic copepods overestimated the biomass. Biomass values using the ESD in LM relationships underestimated the biomass in both taxa, which was expected as the ESD was often smaller than the actual PL of the specimens (Supporting Information Fig. S2). We also tested species-specific CFs for *Calanus* spp. to estimate biomass, which overestimated the biomass greatly in *C. hyperboreus*. In *C. finmarchicus/glacialis*, the biomass values also overestimate the measured biomass, but to a lesser extent (Fig. 6).

Based on the results for *Calanus* spp. as a major contributor to biomass in the Fram Strait, we calculated total zooplankton biomass both using LM relationships based on body length
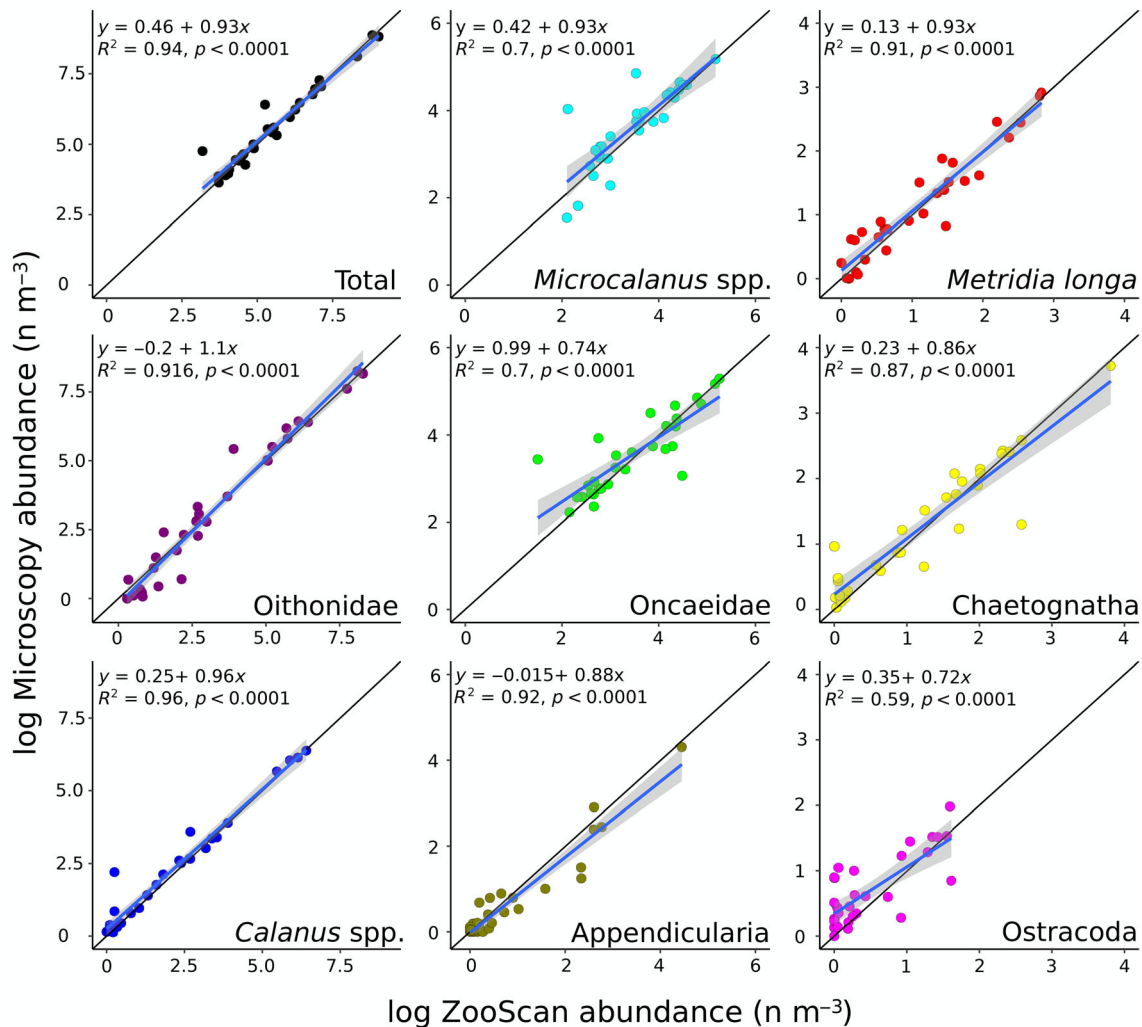
Fig. 4. Correlations between ZooScan and microscopy derived abundances for all samples of the six stations for selected taxa. Black line represents a ratio of 1 : 1; blue line represents the significant relationships; gray areas represent standard errors. The scales vary with the abundances of the respective taxon or group.

and using a general CF for Arctic copepods (Table 8). The total zooplankton biomass (0 to bottom depth/1500 m) ranged between 1.7/2.5 g DM m^{-2} (LM/CF) and 19/24 g DM m^{-2}. To account for the different bottom depths and for comparison with previously published data, total zooplankton biomass was also calculated for the upper 500 m (Table 8). The lowest biomasses were found at the Stas. 71 and 75 in western Fram Strait (LM). The Stas. 54 and 44 in central Fram Strait yielded the highest biomass values, while the eastern Fram Strait Stas. 39 and 127 showed intermediate biomasses.

Normalized biomass size spectra

NBSS of zooplankton were obtained for all depth strata (0–50–200–500–1000–1500 m depth). In all samples, small-sized organisms dominated, however, the steepness of the NBSS slopes differed greatly among the stations in the surface layer

(0–50 m) (Table 9; Fig. 7), while they became more aligned with depth. In the 1000–1500 m intervals, the slopes were congruent, varying between −0.51 and −0.69. In the surface layer, the slope was steepest at Stas. 44, 54, and 127 (−0.76 to −1.1), while it was shallower at the Stats. 71, 75, and 39 (−0.43 to −0.54). These shallower slopes corresponded with the occurrence of biovolume peaks in larger size classes (Fig. 7). At the Stas. 71 and 75, the peak occurred at the largest biovolume size classes that were mainly comprised of CV stages and females of *C. hyperboreus*. At the Stas. 39, 44, 54, and 127, the intermediate peaks in the NBSS plots corresponded to the biovolume size classes of CV stages and females of *C. finmarchicus/glacialis* (Fig. 7). Peaks of larger biovolume size classes corresponding to abundant CV stages and females *C. finmarchicus/glacialis* occurred also in 50–200 m at Stas. 127, 44, 39 and in 500–1000 m depth at
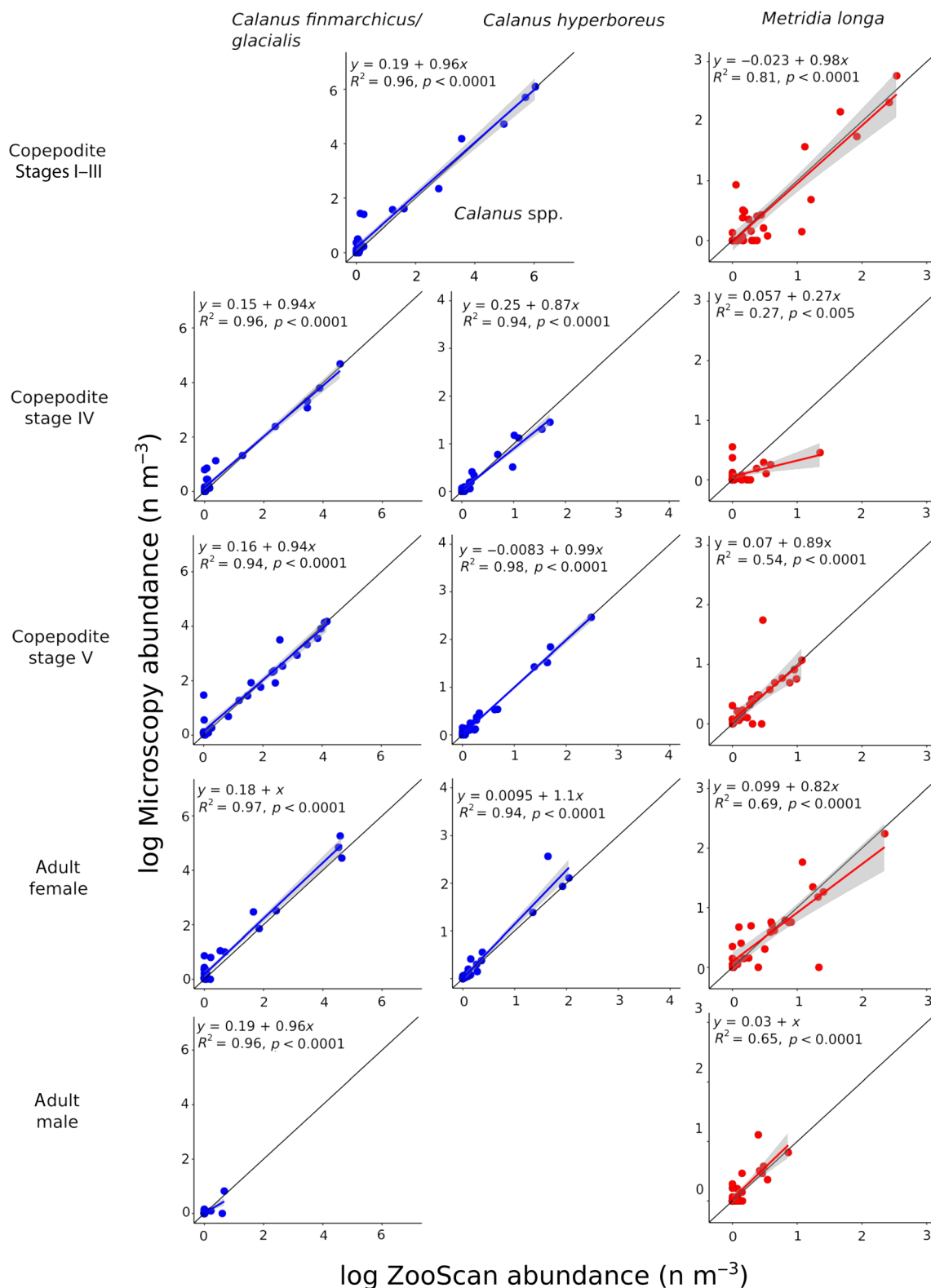
Fig. 5. Linear relationship of abundances (ind m^{-3}) derived from ZooScan and microscopy for the developmental stages of *Calanus finmarchicus/Calanus glacialis*, *Calanus hyperboreus* and *Metridia longa*; from left to right: copepodite stages 1–3 (CI–CIII), 4 (CIV), 5 (CV), females (F), and males (M). Black line represents a ratio of 1 : 1; blue lines represent significant relationships; gray areas represent standard errors.
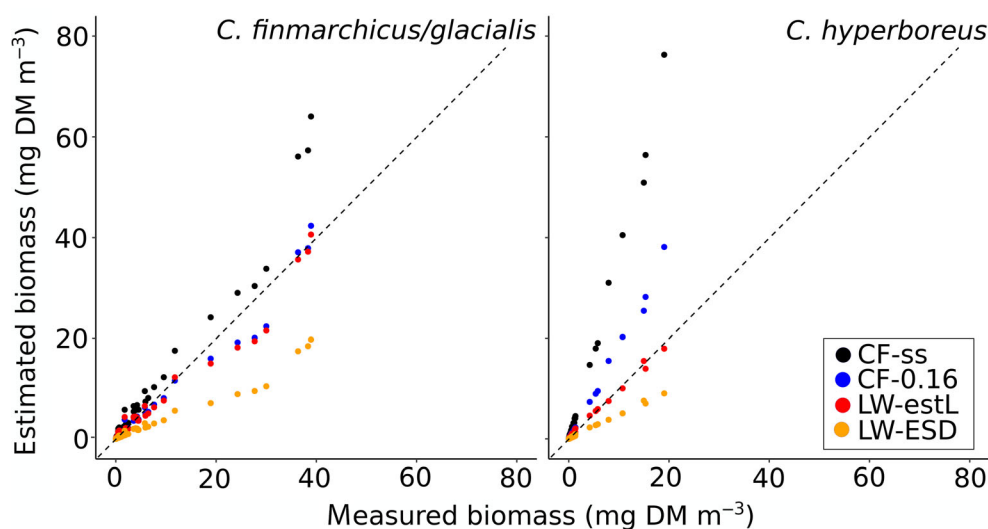
Fig. 6. Comparison of biomass estimates of *Calanus finmarchicus/Calanus glacialis* and *Calanus hyperboreus* with direct measurements of biomass (mg DM m^{-3}). Biomass estimates were calculated with species-specific *Calanus* CFs (CF-ss), with a general Arctic copepod CF of 0.16, with LM relationships based on the estimated length (body length [mm]), and based on the ESD (mm).

Table 8. Total zooplankton biomass (g DM m^{-2}) over the entire sampling depth (0 - bottom/1500 m) and in the upper 500 m (0–500 m), calculated with CFs from WM to DM and with LM relationships based on the estimated body length.

| | Total biomass (g DM m^{-2}) | | | |
| | 0 to bottom/1500 m | | 0–500 m | |
Station	CF	LM	CF	LM
71	2.50	1.67	2.33	1.57
75	5.58	2.91	4.03	2.14
54	24.19	19.05	17.07	13.65
44	23.11	15.31	12.28	11.12
39	13.22	8.78	8.75	7.01
127	12.70	11.33	7.84	7.01

Stas. 127 and 44. In the depth interval 200–500 m, the biomass peaks coincided with the size class of the abundant CV stage and adults of *M. longa* (Stas. 127, 39, 44, 54).

Discussion

In general, our results show that image-based zooplankton quantification in the Arctic Ocean can be used in combination with microscopic analysis and can accelerate future sample analysis for monitoring purposes in the Arctic Ocean (Naito et al. 2019, Romagnon et al. 2016).

Method comparison

This study, to our knowledge, is the 1st that compared results from microscopic and image analyses of preserved samples from the Arctic, addressing zooplankton communities from different water masses and depths. Our data show that the slopes of the linear regressions of abundances determined by microscopy vs. abundances determined with the ZooScan (all data combined) were close to one (0.86–1.1) in total zooplankton abundance and in many of the taxa, and the explanatory power of the regressions was mostly high ($R^2 > 0.9$), indicating that image analysis matched microscopy surprisingly well. Similar horizontal and vertical distribution patterns, hence, emerged from both approaches. Abundances were high in surface waters and decreased with depth, as to be expected (Auel and Hagen 2002; Blachowiak-Samolyk et al. 2007; Gluchowska et al. 2017), and abundances in the upper 50 m were higher in Atlantic waters in eastern and central Fram Strait than in Arctic waters in western Fram Strait. The decline in abundance and biomass from Atlantic to Arctic surface waters is well established (Mumm et al. 1998).

Copepods, dominating in most samples, were comparably easy to identify to at least family levels on images, and—consequently—there were usually only small deviations (less than 5%) between the results from microscopy and image analysis. As to be expected, the total number of copepods that could be assigned to lower taxonomic levels was higher with microscopy than with image analysis. Under the microscope, all copepods were identified to at least family level, whereas on images between 3% and 18% (average: 9.4%) of the copepod specimens in the samples could only be assigned to the general category "copepods". The majority of these organisms were of 0.15–0.3 mm length and in such small specimen, the pixel resolution of 10.6 μm of the ZooScan (Gorsky et al. 2010) limited the taxonomic classification. Most likely, they were younger copepodite stages of *Oithona*, Oncaeidae or *Microcalanus*, and, thus, the total abundances of these taxa

Table 9. Linear regression parameters for NBSS for the standard depth strata at all six stations across Fram Strait.

Depth (m)	Intercept	Slope	R^2	p	Intercept	Slope	R^2	p
		Sta. 71					Sta. 75		
0–50	3.3	−0.54	0.65	<0.001	3.8	−0.54	0.52	<0.01
50–200	0.29	−0.73	0.84	<0.001	−1.5	−0.83	0.70	<0.01
200–500	2.5	−0.54	0.88	<0.001	−0.16	−0.77	0.86	<0.001
500–600/1000	0.16	−0.69	0.84	<0.001	−0.2	−0.74	0.88	<0.001
1000–1500					1.3	−0.62	0.96	<0.001
		Sta. 54					Sta. 44		
0–50	5.0	−0.76	0.84	<0.001	4.6	−0.94	0.87	<0.001
50–200	2.2	−0.87	0.91	<0.001	1.6	−0.80	0.74	<0.001
200–500	4.4	−0.54	0.79	<0.001	4.4	−0.49	0.65	<0.001
500–1000	2.5	−0.68	0.88	<0.001	2.8	−0.55	0.79	<0.001
1000–1500	2.8	−0.57	0.84	<0.001	2.4	−0.51	0.87	<0.001
		Sta. 39					Sta. 127		
0–50	5.7	−0.43	0.56	<0.01	3.2	−1.1	0.87	<0.001
50–200	2.2	−0.64	0.74	<0.001	2.1	−0.94	0.91	<0.001
200–500	3.0	−0.54	0.83	<0.001	3.1	−0.67	0.80	<0.001
500–1000/900	2.8	−0.41	0.83	<0.001	3.7	−0.64	0.87	<0.001
1000–1500	1.8	−0.56	0.95	<0.001				
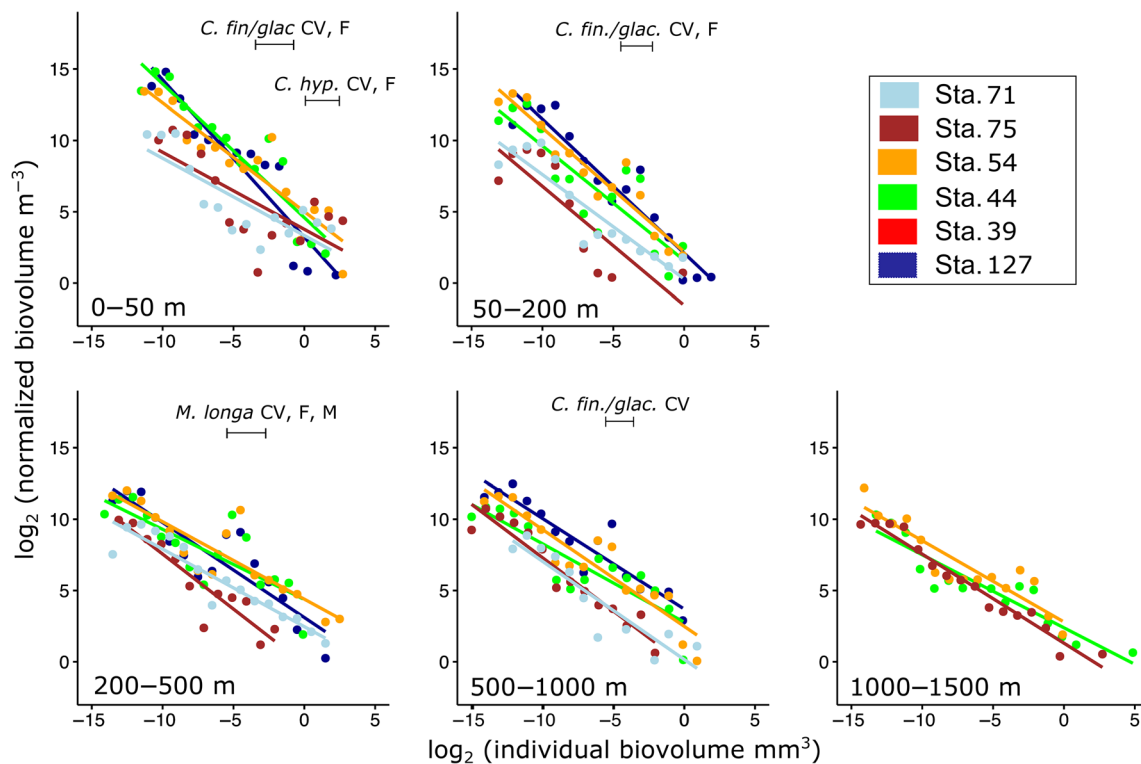
Fig. 7. NBSS for the standard depth strata on all six stations across Fram Strait. Log$_2$ normalized total biovolume (*y*) is plotted against the log$_2$ individual biovolume (*x*). In each depth stratum, the six single spectra for each station are color-coded (*see* legend). For each NBSS, slope, intercept, linear fit (R^2), and level of significance (*p* value) have been calculated (Table 9). The biovolume ranges of the CV stages (CV), females (F), or males (M) of *Calanus finmarchicus/Calanus glacialis* (*C. fin./glac.*), *Calanus hyperboreus* (*C. hyp.*), and *Metridia longa* (*M. longa*) are indicated.

were underestimated by image analysis. In some non-copepod taxa, the abundances varied between the two methods stronger than in copepods: Echinoderm larvae and mollusks can be easily identified on ZooScan images (pers. obs.). However, in our reanalysis of the samples from Fram Strait, their numbers were considerably lower as compared to microscopy results, likely due to sample preservation rather than due to image processing issues. We believe that the carbonate shells/skeletons of these organisms have dissolved during the 8 years of storage. Without their stabilizing carbonate parts, it is hardly possible to recognize these taxa, either under the microscope or on images. We thus recommend to analyze samples quickly after collection or meticulously monitor the pH during extended storage. Moreover, in other non-copepod taxa, such as ostracods, specimens were rare, and deviations in count numbers from small aliquots could have led to large relative differences, when calculating abundances. Nevertheless, the linear regressions of abundance determined by microscopy vs. image analysis were significant in all larger taxa. Therefore, we suggest that image analysis can readily be applied in monitoring programs and large sampling campaigns, allowing faster processing of large numbers of samples. Due to the consistency of data, we also believe that we can combine microscopic data with new (future) image-based data from preserved samples.

The processing of the samples and data benefit from modifications, helping to achieve consistency between abundances determined by microscopy and image analysis. We, 1st, size-fractionated each sample in two sub-samples of organisms larger and smaller than 500 μm, which provided better scans (less overlapping specimens) of larger aliquots than would have been possible with sub-samples of the entire sample. Such an approach may be helpful for all samples, in which the sizes of the zooplankton organisms differ considerably. Second, we stained the small size fraction with Bengal rose which made small organisms much better visible on images. Only then, it was possible to clearly distinguish between detritus and animals, mostly copepods. Third, since the standard minimum ESD (Gorsky et al. 2010) discharged all organisms smaller than 300 μm on the original scan (see Supporting Information Fig. S1), we set the minimum ESD in ZooProcess to 150 μm, which reflected the mesh size used for sampling. This yielded, as to be expected, a higher number of zooplankton organisms, matching the total numbers as determined by microscopy. In order to capture the same size range as in microscopic analyses, we therefore recommend for future ZooScan studies to take the net mesh size into account and choose the ESD threshold in ZooProcess accordingly.

With regard to the taxonomic composition, it has previously been acknowledged that the resolution using imaging techniques is lower as compared to microscopy (Gorsky et al. 2010; Romagnan et al. 2016; Naito et al. 2019). Our study in the Fram Strait, however, revealed that not only the abundances, but also the taxonomic compositions were

largely consistent. Due to the strong dominance of copepods in our samples, a prerequisite for high taxonomic resolution was to determine these specimens to species or at least genera. In temperate and subtropical regions, where most ZooScan studies have been conducted, this is difficult, since the copepod diversity is high (Romagnan et al. 2016; Benedetti et al. 2019; Brandão et al. 2021), and shape and size of the abundant copepod species are similar. In the Arctic, however, we have the advantages that (i) the morphology differs greatly among abundant copepod species, (ii) usually only one or few species per genus or family occur, and (iii) the zooplankton species are often larger as compared to their boreal counterparts, all of which simplifies the identification of species or genera on images.

Semi-automatic determination of copepodite stage of *Calanus* spp. and *M. longa*

The large size of some of the calanoid copepod species in Fram Strait allowed to even distinguish among copepodite stages which, to our knowledge, is a 1st in ZooScan analyses. In our samples, *Calanus* spp. and *M. longa* were sufficiently abundant to present and statistically compare data from image and microscopic analyses. We also separated other calanoid genera and species into females, males and copepodite stages (e.g., Euchaetidae, Aetideidae, Heterorhabdidae, *Pseudocalanus* spp., *Microcalanus* spp.). This implicates that ZooScan images can also be used—at least to some extent—for population dynamics studies in Arctic copepods.

Schmid et al. (2016) developed machine learning algorithms to differentiate between the stages of *Calanus* and *Metridia* spp. on high-resolution images from the optical system Lightframe insight Key species Investigations (Schulz et al. 2010). We, however, used a semi-automatic process, combining manual classification and the automatic algorithms provided by EcoTaxa (Picheral et al. 2017). First, we manually sorted the respective images into two categories, that is, *Metridia* and *Calanus* spp., since the automatic prediction did not reliably separate these two genera. In a 2nd step, we created a learning set with approximately 100 individuals for each juvenile and adult stage of *M. longa* and the 3 *Calanus* species to automatically predict the remaining images. For *M. longa*, we received an accuracy of 94% with the Random Forest classification by EcoTaxa, which was higher than in Schmid et al. (2016). In *Calanus* spp., however, it is more difficult to (automatically) identify the specimens. One reason is that the developmental stages of the three species overlap greatly in size. Thus, the algorithms developed by Schmid et al. (2016, 2018) grouped, for example, C3 *C. finmarchicus* with C2 of *C. glacialis* and C1 of *C. hyperboreus*. Also, in *C. finmarchicus* and *C. glacialis*, each developmental stage may overlap in size, especially at the boundary of their geographic distributions (Choquet et al. 2018). Thus, ideally, molecular samples would have complemented the preserved samples, but were not available for our study. We therefore had to rely

on the traditional approach, distinguishing the three species based on the PLs of their juvenile and adult stages (Unstad and Tande 1991; Hirche et al. 1994; Madsen et al. 2001; Kwasniewski et al. 2003). The developmental stages of *C. hyperboreus* are usually considerably larger than those of the other two species (Madsen et al. 2001), and thus it was easy to identify this species, both under the microscope and on images, often without actually measuring the PLs of the specimens. To distinguish between *C. glacialis* and *C. finmarchicus*, however, more precise length data were necessary. We, therefore, measured all individuals studied under the microscope with ocular scales, yielding only low abundances of *C. glacialis*, when applying published species size ranges. On the more than 11,000 images, manual measurements, for example in ImageJ, would have been very time consuming. We therefore explored the possibility of using the linear relationships between ESD and PL of *C. finmarchicus/glacialis* as developed for biomass calculations. Corresponding to the microscopic length measurements (Thomisch 2012), the length–frequency distribution derived from the ESDs also yielded only few *C. glacialis*, and we presented the data for *C. glacialis* and *C. finmarchicus* combined (i.e., *C. finmarchicus/glacialis*). Our data suggest, however, that the automatic measurement of the ESD provided by EcoTaxa allows to separate the two species with the same accuracy as manually measuring the PLs of the individuals. In monitoring studies, with large amounts of samples, the size-based identification of the three species via image analyses could thus provide the fastest and least expensive estimate of *Calanus* species contributions. For validating the taxonomy based on size, accompanying molecular studies would, however, be necessary.

Comparison of methods to calculate biomass

Ideally, frozen samples for biomass determination, corresponding to samples for zooplankton counts, should be taken during each cruise. This, however, is rarely possible due to constraints in ship time, manpower and, if single species should be sorted, taxonomic expertise onboard. To overcome those obstacles, established LM relationships and CFs from WM to DM have been used in studies on Arctic Ocean zooplankton (Ikeda and Skjoldal 1989; Hirche and Mumm 1992; Richter 1994; Kosobokova and Hirche 2000).

Several methods have been described that estimate biomass from body size or body area derived from zooplankton images (Lehette and León 2009; Pitois et al. 2021; Maas et al. 2021a). In the Arctic, however, such studies have yet been lacking, and our study, to our knowledge, is the 1st comparing image-based approaches in zooplankton from Fram Strait. For *Calanus* spp., we compared the biomass estimates derived from image parameters to measured biomass. To explore the influence of different length measures, we used both the automatically calculated ESD and manually measured body and prosome (copepods) length. As expected, the ESD values were usually lower than the measured lengths, and consequently,

also the biomass values based on ESD were the lowest. We therefore believe that using only ESDs underestimates the biomass, and we recommend to 1st relate ESDs to measured body lengths even though this approach is more time consuming (Matsuno and Yamaguchi 2010).

In addition to LM relationships, general CFs that translate biovolume (WM) into DM have been applied (Ikeda and Skjoldal 1989; Kosobokova and Hirche 2000; Postel et al. 2000). Ikeda and Skjoldal (1989) suggested also taxon-specific CFs for *Calanus* spp. When we applied these specific CFs, they yielded higher biomass values for *Calanus* spp. at all stations and depths in the present study than any other method. Using a general WM to DM CF for Arctic copepods of 0.16 (Kosobokova and Hirche 2000) yielded *Calanus* spp. biomass values comparable to direct measurements of DM for *C. finmarchicus/glacialis*, but underestimated that of *C. hyperboreus*.

Our estimates of total zooplankton biomass across Fram Strait show a similar range using either LM relationships and CFs, varying between 1.7 and 19 g DM m^{-2} for LM relationships and from 2.5 to 24 g DM m^{-2} using CFs. In eastern Fram Strait, Blachowiak-Samolyk et al. (2007) found that biomass varied between 4.3 and 24.4 g DM m^{-2} at deep-sea stations. However, their calculations were based on mean species-specific DM data taken from previous published studies. In the Canadian Basin, zooplankton biomass ranged between 7.3 and 12.8 g DM m^{-2} in the upper 500 m based on DM measurements (Thibault et al. 1999). These results show that our biomass estimates both based on LM relationships and converted from biovolume provide realistic values of zooplankton biomass in the Arctic Ocean. However, further calibration with direct measurements is still advisable.

Size spectra

Body size is an ecological trait, relatively easy to obtain and an indicator for ecosystem status (Atkinson et al. 2021) and alterations in the food-web structure (Gorokhova et al. 2016). In the Arctic Ocean, a size-based analysis could be an important supplement in long-term studies to monitor changes due to climate warming (Trudnowska et al. 2020), and would enable a rapid assessment of the status of the pelagic ecosystem. However, only few studies have yet used this approach. In the Arctic, biomass size spectra have been investigated based on Laser Optical Plankton Counter (Basedow et al. 2010), Optical Plankton Counter (Matsuno et al. 2012; Naito et al. 2019), and digital microscope photographs (Trudnowska et al. 2020). In contrast to the OPC and LOPC analyses, non-living particles such as detritus, silt, and others can be removed from the ZooScan data set during the analysis and, thus, may provide a closer estimate of zooplankton biomass (Naito et al. 2019). Digital microscopic photographs on the other hand provide detailed information on body size, but are more time-consuming than ZooScan analyses.

Although previous studies on size spectra in the Arctic Ocean were obtained only from epipelagic layers, we plotted biomass size spectra in 5 depth layers down to 1500 m. The NBSS plots revealed that communities in the warm surface layer of Atlantic-influenced stations (Stas. 54, 44, and 127) had steeper NBSS slopes, corroborated by high chlorophyll *a* (Chl *a*) concentration (Nöthig et al. 2015) and high zooplankton abundances. NBSS plots of surface communities at stations with Polar Surface Water (stns. 71, 75, and 39) had more gentle slopes, corroborated by low Chl *a* concentrations and low zooplankton abundances (Nöthig et al. 2015). Our findings correspond with the differences found in Arctic and Atlantic surface waters in the Barents Sea (Basedow et al. 2010).

NBSS derived from automatic size measurements can also provide some information on the occurrence of specific species or genera: In our NBSS, the presence of different *Calanus* species was visible in the moderate NBSS slopes. In the Polar Surface Water at Stas. 71 and 75, high abundance of older developmental stages of *C. hyperboreus* caused the shallow slopes. At other stations, high abundances of *C. finmarchicus/ glacilis* also were indicative of shallower slopes. This could be useful when monitoring the same ecosystem over time and tracking vertical migration behavior of dominant Arctic zooplankton species.

Our study shows that ZooScan analyses can be a very good alternative to the microscopy of zooplankton samples from Arctic ecosystems, since not only abundance and taxonomic composition, but also the population structure of large key species was comparable between the two methods. Such consistency allows the combination of historic (microscopic) data with ZooScan image analysis for long-term monitoring purposes. Furthermore, the ZooScan analysis allows a rapid assessment of biomass and size structure of zooplankton communities. The differences in biomass and size spectra between Polar and Atlantic surface waters, as observed in our study, suggest that these measures may become important for studying climate change induced community shifts in the Arctic. Furthermore, it will allow us to estimate biomass and size taxon-specific respiration rates (Ikeda 2014; Bode et al. 2018; Kiko and Hauss 2019; Maas et al. 2021b) to assess the role of zooplankton in the pelagic Arctic biogeochemical cycle.

References

Alcaraz, M., and others. 2010. The role of arctic zooplankton in biogeochemical cycles: Respiration and excretion of ammonia and phosphate during summer. Polar Biol. **33**: 1719–1731. doi:10.1007/s00300-010-0789-9

Andersen, K. H., and others. 2015. Characteristic sizes of life in the oceans, from bacteria to whales. Ann. Rev. Mar. Sci. **8**: 1–25. doi:10.1146/annurev-marine-122414-034144

Atkinson, A., and others. 2021. Increasing nutrient stress reduces the efficiency of energy transfer through planktonic size spectra. Limnol. Oceanogr. **66**: 422–437. doi:10.1002/lno.11613

Auel, H., and W. Hagen. 2002. Mesozooplankton community structure, abundance and biomass in the central Arctic Ocean. Mar. Biol. **140**: 1013–1021. doi:10.1007/s00227-001-0775-4

Auel, H., and I. Werner. 2003. Feeding, respiration and life history of the hyperiid amphipod *Themisto libellula* in the Arctic marginal ice zone of the Greenland Sea. J. Exp. Mar. Biol. Ecol. **296**: 183–197. doi:10.1016/s0022-0981(03)00321-6

Basedow, S. L., K. S. Tande, and M. Zhou. 2010. Biovolume spectrum theories applied: Spatial patterns of trophic levels within a mesozooplankton community at the polar front. J. Plankton Res. **32**: 1105–1119. doi:10.1093/plankt/fbp110

Benedetti, F., and others. 2019. The seasonal and inter-annual fluctuations of plankton abundance and community structure in a North Atlantic marine protected area. Front. Mar. Sci. **6**: 214. doi:10.3389/fmars.2019.00214

Benfield, M. C., and others. 2007. RAPID: Research on automated plankton identification. Oceanography **20**: 172–187. doi:10.1371/journal.pone.0127121

Beszczynska-Möller, A., E. Fahrbach, U. Schauer, and E. Hansen. 2012. Variability in Atlantic water temperature and transport at the entrance to the Arctic Ocean, 1997–2010. ICES J. Mar. Sci. **69**: 852–863. doi:10.1093/icesjms/fss056

Beszczynska-Möller, A., and A. Wisotzki. 2012. Physical oceanography during POLARSTERN cruise ARK-XXVI/1. Alfred Wegener Institute, Helmholtz Centre for Polar and Marine Research, PANGAEA. doi:10.1594/pangaea.774196

Blachowiak-Samolyk, K., S. Kwasniewski, K. Dmoch, H. Hop, and S. Falk-Petersen. 2007. Trophic structure of zooplankton in the Fram Strait in spring and autumn 2003. J. Exp. Mar. Biol. Ecol. **54**: 2716–2728. doi:10.1016/j.dsr2.2007.08.004

Bode, M., R. Koppelmann, L. Teuber, W. Hagen, and H. Auel. 2018. Carbon budgets of mesozooplankton copepod communities in the eastern Atlantic Ocean—Regional and vertical patterns between 24°N and 21°S. Global Biogeochem. Cycl. **32**: 840–857. doi:10.1029/2017gb005807

Brandão, M. C., and others. 2021. Macroscale patterns of oceanic zooplankton composition and size structure. Sci. Rep. **11**: 15714. doi:10.1038/s41598-021-94615-5

Brun, P., M. R. Payne, and T. Kiørboe. 2017. A trait database for marine copepods. Earth Syst. Sci. Data **9**: 99–113. doi:10.5194/essd-9-99-2017

Calbet, A., and E. Saiz. 2005. The ciliate-copepod link in marine ecosystems. Aquat. Microb. Ecol. **38**: 157–167. doi:10.3354/ame038157

Choquet, M., and others. 2018. Can morphology reliably distinguish between the copepods *Calanus finmarchicus* and *C. glacialis*, or is DNA the only way? Limnol. Oceanogr. Methods **16**: 237–252. doi:10.1002/lom3.10240

Cornils, A., K. Thomisch, J. Hase, N. Hildebrandt, H. Auel, and B. Niehoff. 2022. Abundance, biovolume, biomass and length measurements of mesozooplankton from the POLARSTERN cruise PS78 (ARK‐XXVI/1). PANGAEA. doi:10.1594/PANGAEA.944235

Cornils, A. 2022. Zooplankton abundance and biomass from ZooScan images (v1.0.1). Zenodo. doi:10.5281/zenodo.6552614

Darnis, G., and L. Fortier. 2012. Zooplankton respiration and the export of carbon at depth in the Amundsen Gulf (Arctic Ocean). J. Geophys. Res. **117**: C04013. doi:10.1029/2011jc007374

Daufresne, M., K. Lengfellner, and U. Sommer. 2009. Global warming benefits the small in aquatic ecosystems. Proc. Nat. Acad. Sci. **106**: 12788–12793. doi:10.1073/pnas.0902080106

Fenaux, R. 1976. Cycle vital d'un appendiculaire: Oikopleura dioica Fol, 1872. Description et chronologie. Ann. Inst. Oceanogr. Paris. **52**: 89–101.

Fossheim, M., R. Primicerio, E. Johannesen, R. B. Ingvaldsen, M. M. Aschan, and A. V. Dolgov. 2015. Recent warming leads to a rapid borealization of fish communities in the Arctic. Nat. Clim. Change **5**: 673–677. doi:10.1038/nclimate2647

García-Comas, C., C.-Y. Chang, L. Ye, A. R. Sastri, Y.-C. Lee, G.-C. Gong, and C. Hsieh. 2014. Mesozooplankton size structure in response to environmental conditions in the East China Sea: How much does size spectra theory fit empirical data of a dynamic coastal area? Prog. Oceanogr. **121**: 141–157. doi:10.1016/j.pocean.2013.10.010

Gluchowska, M., P. Dalpadado, A. Beszczynska-Möller, A. Olszewska, R. B. Ingvaldsen, and S. Kwasniewski. 2017. Interannual zooplankton variability in the main pathways of the Atlantic water flow into the Arctic Ocean (Fram Strait and Barents Sea branches). ICES J. Mar. Sci. **74**: 1921–1936. doi:10.1093/icesjms/fsx033

Gorokhova, E., and others. 2016. Indicator properties of Baltic zooplankton for classification of environmental status within marine strategy framework directive. PLos One **11**: e0158326. doi:10.1371/journal.pone.0158326

Gorsky, G., and others. 2010. Digital zooplankton image analysis using the ZooScan integrated system. J. Plankton Res. **32**: 285–303. doi:10.1093/plankt/fbp124

Grosjean, P., M. Picheral, C. Warembourg, and G. Gorsky. 2004. Enumeration, measurement, and identification of net zooplankton samples using the ZOOSCAN digital imaging system. ICES J. Mar. Sci. **61**: 518–525. doi:10.1016/j.icesjms.2004.03.012

Heneghan, R. F., and others. 2020. A functional size-spectrum model of the global marine ecosystem that resolves zooplankton composition. Ecol. Model. **435**: 109265. doi:10.1016/j.ecolmodel.2020.109265

Hirche, H. J., and N. Mumm. 1992. Distribution of dominant copepods in the Nansen Basin, Arctic Ocean, in summer. Deep-Sea Res. **39**: S485–S505. doi:10.1016/s0198-0149(06)80017-8

Hirche, H. J., W. Hagen, N. Mumm, and C. Richter. 1994. The northeast water polynya, Greenland Sea. Polar Biol. **14**: 491–503. doi:10.1007/bf00239054

Hopcroft, R. R., C. Clarke, R. J. Nelson, and K. A. Raskoff. 2004. Zooplankton communities of the Arctic's Canada Basin: The contribution by smaller taxa. Polar Biol. **28**: 198–206. doi:10.1007/s00300-004-0680-7

Ikeda, T. 2014. Respiration and ammonia excretion by marine metazooplankton taxa: Synthesis toward a global-bathymetric model. Mar. Biol. **161**: 2753–2766. doi:10.1007/s00227-014-2540-5

Ikeda, T., and H. R. Skjoldal. 1989. Metabolism and elemental composition of zooplankton from the Barents Sea during early Arctic summer. Mar. Biol. **100**: 173–183. doi:10.1007/bf00391956

Kiko, R., and H. Hauss. 2019. On the estimation of zooplankton-mediated active fluxes in oxygen minimum zone regions. Front. Mar. Sci. **6**: 741. doi:10.3389/fmars.2019.00741

Kiørboe, T. 2013. Zooplankton body composition. Limnol. Oceanogr. **58**: 1843–1850. doi:10.4319/lo.2013.58.5.1843

Kiørboe, T., and A. G. Hirst. 2014. Shifts in mass scaling of respiration, feeding, and growth rates across life-form transitions in marine pelagic organisms. Am. Nat. **183**: E118–E130. doi:10.1086/675241

Kosobokova, K., and H. J. Hirche. 2000. Zooplankton distribution across the Lomonosov Ridge, Arctic Ocean: Species inventory, biomass and vertical structure. J. Exp. Mar. Biol. Ecol. **47**: 2029–2060. doi:10.1016/s0967-0637(00)00015-7

Kwasniewski, S., H. Hop, S. Falk-Petersen, and G. Pedersen. 2003. Distribution of *Calanus* species in Kongsfjorden, a glacial fjord in Svalbard. J. Plankton Res. **25**: 1–20. doi:10.1093/plankt/25.1.1

Kwok, R. 2018. Arctic Sea ice thickness, volume, and multiyear ice coverage: Losses and coupled variability (1958-2018). Environ. Res. Lett. **13**: 105005. doi:10.1088/1748-9326/aae3ec

Lampe, V., E.-M. Nöthig, and M. Schartau. 2021. Spatio-temporal variations in community size structure of Arctic Protist plankton in the Fram Strait. Front. Mar. Sci. **7**: 579880. doi:10.3389/fmars.2020.579880

Le Quéré, C., and others. 2016. Role of zooplankton dynamics for Southern Ocean phytoplankton biomass and global biogeochemical cycles. Biogeosciences **13**: 4111–4133. doi:10.5194/bg-13-4111-2016

Lehette, P., and S. H. León. 2009. Zooplankton biomass estimation from digitized images: A comparison between subtropical and Antarctic organisms. Limnol. Oceanogr. Methods **7**: 304–308. doi:10.4319/lom.2009.7.304

Litchman, E., M. D. Ohman, and T. Kiørboe. 2013. Trait-based approaches to zooplankton communities. J. Plankton Res. **35**: 473–484. doi:10.1093/plankt/fbt019

Liu, H., and R. Hopcroft. 2008. Growth and development of *Pseudocalanus* spp. in the northern Gulf of Alaska. J. Plankton Res. **30**: 923–935. doi:10.1093/plankt/fbn046

Lombard, F., and others. 2019. Globally consistent quantitative observations of planktonic ecosystems. Front. Mar. Sci. **6**: 196. doi:10.3389/fmars.2019.00196

Longhurst, A. R., and W. G. Harrison. 1988. Vertical nitrogen flux from the oceanic photic zone by diel migrant zooplankton and nekton. Deep Sea Res. **35**: 881–889. doi:10.1016/0198-0149(88)90065-9

Maas, A. E., H. Gossner, M. J. Smith, and L. Blanco-Bercial. 2021a. Use of optical imaging datasets to assess biogeochemical contributions of the mesozooplankton. J. Plankton Res. **43**: 475–491. doi:10.1093/plankt/fbab037

Maas, A. E., A. Miccoli, K. Stamieszkin, C. A. Carlson, and D. K. Steinberg. 2021b. Allometry and the calculation of zooplankton metabolism in the subarctic Northeast Pacific Ocean. J. Plankton Res. **43**: 413–427. doi:10.1093/plankt/fbab026

Madsen, S. D., T. G. Nielsen, and B. W. Hansen. 2001. Annual population development and production by *Calanus finmarchicus*, *C. glacialis* and *C. hyperboreus* in Disko Bay, western Greenland. Mar. Biol. **139**: 75–93. doi:10.1007/s002270100552

Matsuno, K., and A. Yamaguchi. 2010. Abundance and biomass of mesozooplankton along north-south transects (165°E and 165°W) in summer in the North Pacific: An analysis with an optical plankton counter. Plankton Benthos Res. **5**: 123–130. doi:10.3800/pbr.5.123

Matsuno, K., A. Yamaguchi, and I. Imai. 2012. Biomass size spectra of mesozooplankton in the Chukchi Sea during the summers of 1991/1992 and 2007/2008: An analysis using optical plankton counter data. ICES J. Mar. Sci. **69**: 1205–1217. doi:10.1093/icesjms/fss119

Matthews, J., and L. Hestad. 1977. Ecological studies on the deep-water pelagic community of Korsfjorden, Western Norway: Length/weight relationships for some macroplanktonic organisms. Sarsia **63**: 57–63. doi:10.1080/00364827.1977.10411322

Mitra, A., and others. 2014. Bridging the gap between marine biogeochemical and fisheries sciences; configuring the zooplankton link. Prog. Oceanogr. **129**: 176–199. doi:10.1016/j.pocean.2014.04.025

Mizdalski, E. 1988. Weight and length data of zooplankton in the Weddell Sea in austral spring 1986 (ANT V/3). Rep. Polar Mar. Res. **55**: 1–72. doi:10.2312/BzP_0055_1988

Møller, E., P. Thor, and T. Nielsen. 2003. Production of DOC by *Calanus finmarchicus*, *C. glacialis* and *C. hyperboreus* through sloppy feeding and leakage from fecal pellets. Mar. Ecol. Prog. Ser. **262**: 185–191. doi:10.3354/meps262185

Møller, E. F. 2005. Sloppy feeding in marine copepods: Prey-size-dependent production of dissolved organic carbon. J. Plankton Res. **27**: 27–35. doi:10.1093/plankt/fbh147

Møller, E. F., and T. G. Nielsen. 2019. Borealization of Arctic zooplankton—Smaller and less fat zooplankton species in Disko Bay, Western Greenland. Limnol. Oceanogr. **65**: 1175–1188. doi:10.1002/lno.11380

Muilwijk, M., L. H. Smedsrud, M. Ilicak, and H. Drange. 2018. Atlantic water heat transport variability in the 20th century Arctic Ocean from a Global Ocean model and observations. J. Geophys. Res. Oceans **123**: 8159–8179. doi:10.1029/2018jc014327

Mumm, N. 1991. Zur sommerlichen Verteilung des Mesozooplanktons im Nansen-Becken, Nordpolarmeer. Rep. Polar Mar. Res. **92**: 1–146.

Mumm, N., H. Auel, H. Hanssen, W. Hagen, C. Richter, and H. J. Hirche. 1998. Breaking the ice: Large-scale distribution of mesozooplankton after a decade of Arctic and transpolar cruises. Polar Biol. **20**: 189–197. doi:10.1007/s003000050295

Naito, A., Y. Abe, K. Matsuno, B. Nishizawa, N. Kanna, S. Sugiyama, and A. Yamaguchi. 2019. Surface zooplankton size and taxonomic composition in Bowdoin Fjord, North-Western Greenland: A comparison of ZooScan, OPC and microscopic analyses. Polar Sci. **19**: 120–129. doi:10.1016/j.polar.2019.01.001

Nakamura, A., K. Matsuno, Y. Abe, H. Shimada, and A. Yamaguchi. 2017. Length–weight relationships and chemical composition of the dominant mesozooplankton taxa/species in the subarctic Pacific, with special reference to the effect of lipid accumulation in Copepoda. Zool. Stud. **56**: 1–15. doi:10.6620/zs.2017.56-13

Nöthig, E.-M., and others. 2015. Summertime plankton ecology in Fram Strait—A compilation of long- and short-term observations. Polar Res. **34**: 23349. doi:10.3402/polar.v34.23349

Paquette, R. G., R. H. Bourke, J. F. Newton, and W. F. Perdue. 1985. The East Greenland polar front in autumn. J. Geophys. Res. **90**: 4866–4882. doi:10.1029/JC090iC03p04866

Petchey, O. L., and A. Belgrano. 2010. Body-size distributions and size-spectra: Universal indicators of ecological status? Biol. Lett. **6**: 434–437. doi:10.1098/rsbl.2010.0240

Picheral, M., S. Colin, and J.-O. Irisson. 2017. EcoTaxa, a tool for the taxonomic classification of images. http://ecotaxa.obs-vlfr.fr

Pinchuk, A. I., and R. R. Hopcroft. 2007. Seasonal variations in the growth rates of euphausiids (*Thysanoessa inermis*, *T. spinifera*, and *Euphausia pacifica*) from the northern Gulf of Alaska. Mar. Biol. **151**: 257–269. doi:10.1007/s00227-006-0483-1

Pitois, S. G., C. A. Graves, H. Close, C. Lynam, J. Scott, J. Tilbury, J. van der Kooij, and P. Culverhouse. 2021. A first approach to build and test the copepod mean size and total abundance (CMSTA) ecological indicator using in-situ size measurements from the Plankton Imager (PI). Ecol. Indic. **123**: 107307. doi:10.1016/j.ecolind.2020.107307

Plum, C., A. Cornils, R. Driscoll, P. Wenta, T. H. Badewien, J. Niggelmann, and S. Moorthi. 2021. Mesozooplankton trait

distribution in relation to environmental conditions and the presence of krill and salps along the northern Antarctic Peninsula. J. Plankton Res. **43**: 927–944. doi:10.1093/plankt/fbab068

Polyakov, I. V., and others. 2017. Greater role for Atlantic inflows on sea-ice loss in the Eurasian Basin of the Arctic Ocean. Science **356**: 285–291. doi:10.1126/science.aai8204

Postel, L., H. Fock, and W. Hagen. 2000. Biomass and abundance, p. 83–192. *In* R. Harris and others [eds.], ICES zooplankton methodology manual. Academic Press.

R Core Team. 2021. R: A language and environment for statistical computing. R Foundation for Statistical Computing.

Richter, C. 1994. Regional and seasonal variability in the vertical distribution of mesozooplankton in the Greenland Sea. Rep. Polar Mar. Rese. **154**: 1–96.

Riser, C. W., P. Wassmann, M. Reigstad, and L. Seuthe. 2008. Vertical flux regulation by zooplankton in the northern Barents Sea during Arctic spring. J.Exp. Mar. Biol. Ecol. **55**: 2320–2329. doi:10.1016/j.dsr2.2008.05.006

Romagnan, J. B., L. Aldamman, S. Gasparini, P. Nival, A. Aubert, J.-L. Jamet, and L. Stemmann. 2016. High frequency mesozooplankton monitoring: Can imaging systems and automated sample analysis help us describe and interpret changes in zooplankton community composition and size structure? An example from a coastal site. J. Mar. Syst. **162**: 18–28. doi:10.1016/j.jmarsys.2016.03.013

RStudio Team. 2021. Rstudio: Integrated development for R. Rstudiom Inc..

Schlitzer, R. 2021. Ocean data view vs. 5.3.0. https://odv.awi.de

Schmid, M. S., C. Aubry, J. Grigor, and L. Fortier. 2016. The LOKI underwater imaging system and an automatic identification model for the detection of zooplankton taxa in the Arctic Ocean. Methods Oceanogr. **15–16**: 129–160. doi:10.1016/j.mio.2016.03.003

Schmid, M. S., F. Maps, and L. Fortier. 2018. Lipid load triggers migration to diapause in Arctic *Calanus* copepods—Insights from underwater imaging. J. Plankton Res. **40**: 311–325. doi:10.1093/plankt/fby012

Schnack-Schiel, S. B., and E. Isla. 2005. The role of zooplankton in the pelagic-benthic coupling of the Southern Ocean. Sci. Mar. **69**: 39–55. doi:10.3989/scimar.2005.69s239

Schneider, C. A., W. S. Rasband, and K. W. Eliceiri. 2012. NIH image to ImageJ: 25 years of image analysis. Nat. Methods **9**: 671–675. doi:10.1038/nmeth.2089

Schulz, J., K. Barz, P. Ayon, A. Ludtke, O. Zielinski, D. Mengedoht, and H. J. Hirche. 2010. Imaging of plankton specimens with the lightframe on-sight keyspecies investigation (LOKI) system. J. Eur. Opt. Soc. Rapid **5**: 10017s. doi:10.2971/jeos.2010.10017s

Smetacek, V., and S. Nicol. 2005. Polar ocean ecosystems in a changing world. Nature **437**: 362–368. doi:10.1038/nature04161

Soltwedel, T., and others. 2005. HAUSGARTEN: Multidisciplinary investigations at a deep-sea, long-term observatory in the Arctic Ocean. Oceanography **18**: 46–61. doi:10.5670/oceanog.2005.24

Soltwedel, T., and others. 2016. Natural variability or anthropogenically-induced variation? Insights from 15 years of multidisciplinary observations at the arctic marine LTER site HAUSGARTEN. Ecol. Indic. **65**: 89–102. doi:10.1016/j.ecolind.2015.10.001

Sprules, W. G., and M. Munawar. 1986. Plankton size spectra in relation to ecosystem productivity, size, and perturbation. Can. J. Fish. Aquat. Sci. **43**: 1789–1794. doi:10.1139/f86-222

Sprules, W. G., and L. E. Barth. 2016. Surfing the biomass size spectrum: Some remarks on history, theory, and application. Can. J. Fish. Aquat. Sci. **73**: 477–495. doi:10.1139/cjfas-2015-0115

Stroeve, J. C., M. C. Serreze, M. M. Holland, J. E. Kay, J. Malanik, and A. P. Barrett. 2012. The Arctic's rapidly shrinking sea ice cover: A research synthesis. Clim. Change **110**: 1005–1027. doi:10.1007/s10584-011-0101-1

Swift, J. H., and K. Aagaard. 1981. Seasonal transitions and water mass formation in the Iceland and Greenland seas. Deep Sea Res. **28**: 1107–1129. doi:10.1016/0198-0149(81)90050-9

Thibault, D., E. J. H. Head, and P. A. Wheeler. 1999. Mesozooplankton in the Arctic Ocean in summer. Deep-Sea Res. **46**: 1391–1415. doi:10.1016/s0967-0637(99)00009-6

Thomisch, K. 2012. Mesozooplankton in the Fram Strait: Distribution, abundance and species composition in a warming Arctic Ocean. M.Sc. thesis. Univ. of Bremen.

Trudnowska, E., L. Stemmann, K. Blachowiak-Samołyk, and S. Kwasniewski. 2020. Taxonomic and size structures of zooplankton communities in the fjords along the Atlantic water passage to the Arctic. J. Mar. Syst. **204**: 103306. doi:10.1016/j.jmarsys.2020.103306

Unstad, K. H., and K. S. Tande. 1991. Depth distribution of *Calanus finmarchicus* and *C. glacialis* in relation to environmental conditions in the Barents Sea. Polar Res. **10**: 409–420. doi:10.3402/polar.v10i2.6755

van der Jagt, H., I. Wiedmann, N. Hildebrandt, B. Niehoff, and M. H. Iversen. 2020. Aggregate feeding by the copepods *Calanus* and *Pseudocalanus* controls carbon flux attenuation in the Arctic Shelf Sea during the productive period. Front. Mar. Sci. **7**: 543124. doi:10.3389/fmars.2020.543124

Vandromme, P., and others. 2012. Zooplankton communities fluctuations from 1995 to 2005 in the Bay of Villefranche-Sur-Mer (Northern Ligurian Sea, France). Biogeosci. Discuss. **7**: 9175–9217. doi:10.5194/bgd-7-9175-2010

Villarino, E., and others. 2018. Large-scale ocean connectivity and planktonic body size. Nat. Commun. **9**: 142. doi:10.1038/s41467-017-02535-8

Wassmann, P., and others. 2004. Particulate organic carbon flux to the Arctic Ocean sea floor, p. 101–138. *In* R. Stein and others [eds.], The organic carbon cycle in the Arctic Ocean. Springer. doi:10.1007/978-3-642-18912-8_5

Wickham, H. 2016. ggplot2: Elegant graphics for data analysis. Springer.

Wickham, H., and others. 2019. Welcome to the tidyverse. J. Open Sour. Softw. **4**: 1686. doi:10.21105/joss.01686

Yamaguchi, A., C. J. Ashjian, R. G. Campbell, and Y. Abe. 2020. Vertical distribution, population structure and developmental characteristics of the less studied but globally distributed mesopelagic copepod *Scaphocalanus magnus* in the western Arctic Ocean. J. Plankton Res. **42**: 368–377. doi:10.1093/plankt/fbaa021

Zhou, M. 2006. What determines the slope of a plankton biomass spectrum? J. Plankton Res. **28**: 437–448. doi:10.1093/plankt/fbi119

Conflict of Interest

None declared.